Commun. Comput. Phys.
doi: 10.4208/cicp.OA-2023-0021

Vol. **34**, No. 1, pp. 132-172
July 2023

Random Walk Approximation for Irreversible Drift-Diffusion Process on Manifold: Ergodicity, Unconditional Stability and Convergence

Yuan Gao[1,*] and Jian-Guo Liu[2]

[1] *Department of Mathematics, Purdue University, West Lafayette, IN, USA.*
[2] *Departments of Mathematics and Physics, Duke University, Durham, NC, USA.*

Received 17 January 2023; Accepted (in revised version) 11 April 2023

Abstract. Irreversible drift-diffusion processes are very common in biochemical reactions. They have a non-equilibrium stationary state (invariant measure) which does not satisfy detailed balance. For the corresponding Fokker-Planck equation on a closed manifold, using Voronoi tessellation, we propose two upwind finite volume schemes with or without the information of the invariant measure. Both schemes possess stochastic Q-matrix structures and can be decomposed as a gradient flow part and a Hamiltonian flow part, enabling us to prove unconditional stability, ergodicity and error estimates. Based on the two upwind schemes, several numerical examples – including sampling accelerated by a mixture flow, image transformations and simulations for stochastic model of chaotic system – are conducted. These two structure-preserving schemes also give a natural random walk approximation for a generic irreversible drift-diffusion process on a manifold. This makes them suitable for adapting to manifold-related computations that arise from high-dimensional molecular dynamics simulations.

AMS subject classifications: 60H30, 60H35, 65M75, 65M12

Key words: Symmetric decomposition, non-equilibrium thermodynamics, enhancement by mixture, exponential ergodicity, structure-preserving numerical scheme.

1 Introduction

A general stationary (time-homogeneous) dynamical system with white noise, can be modeled by a stochastic differential equation for $\mathbf{y}_t \in \mathbb{R}^\ell$

$$\mathrm{d}\mathbf{y}_t = \boldsymbol{b}(\mathbf{y}_t)\,\mathrm{d}t + \sqrt{2}\sigma\,\mathrm{d}B_t, \tag{1.1}$$

*Corresponding author. *Email addresses:* gao662@purdue.edu (Y. Gao), jian-guo.liu@duke.edu (J.-G. Liu)

where σ is a noise matrix and B_t is an ℓ-dimensional Brownian motion. Denote $D := \sigma\sigma^T \in \mathbb{R}^{\ell\times\ell}$. For simplicity, we assume D is a constant positive semi-definite matrix. By Ito's formula, SDE (1.1) gives the following Fokker-Planck equation, which is the master equation for the time marginal density $\rho_t(\mathbf{y})$

$$\partial_t\rho = -\nabla\cdot(\boldsymbol{b}\rho) + \nabla\cdot(D\nabla\rho) =: \mathcal{L}^*\rho. \tag{1.2}$$

In some physical systems, the drift vector field $\boldsymbol{b} = -D\nabla\varphi$ for some potential φ representing the energy landscape. Then the Gibbs measure $\pi(\mathbf{y}) \propto e^{-\varphi(\mathbf{y})}$ is the invariant measure. The simplest example is the Ornstein-Uhlenbeck process with $\boldsymbol{b}(\mathbf{y}_t) = -\gamma\mathbf{y}_t$ and the diffusion coefficient $\sigma = \sqrt{\varepsilon\gamma}$. In this case, (1.1) is called Langevin dynamics, and the corresponding Fokker-Planck equation has a gradient flow structure; see (2.22). In this Langevin dynamics case, the Markov process defined by (1.1) is reversible[†], i.e., if we take π as the initial density, the time-reversed process has the same law as that of the forward process. Equivalently, the invariant measure satisfies the detailed balance condition

$$\text{steady flux } F^\pi := -\boldsymbol{b}\pi + D\nabla\pi = 0. \tag{1.3}$$

However, numerous dynamical systems in physics and biochemistry are described by irreversible Markov processes (without detailed balance), i.e., there does *not* exist a potential function such that the drift vector field $\boldsymbol{b} = -D\nabla\varphi$ in (1.1). For instance, the stochastic Lorenz system, the Belousov–Zhabotinsky reaction, or the Hodgkin–Huxley model describe the excitation and propagation of sodium and potassium ions in a neuron. The irreversibility in the nonequilibrium circulation balance is almost literally the primary characteristic of life activities [19]. In this case, the invariant measure π is still stationary in time, but there is a positive entropy production rate; see (3.12). Thus PRIGOGINE named such an invariant measure π as "stationary non-equilibrium states" or "non-equilibrium steady states" in [29, Chapter VI]. We will simply call it steady state or invariant measure. Later, Hill explains Prigogine's theory using Markov chain stochastic models for some simple biochemical reactions such as muscle contraction and clarifies the formula (3.12) for the entropy production rate [19, eq. (9.20)]. Another situation is that for a Markov process on manifold, which is induced via dimension reductions (such as diffusion map [7]) from a higher dimensional Markov process based on collected data, some classical schemes such as the Euler-Maruyama scheme will break the detailed balance property.

Therefore, in this paper we focus on designing numerical schemes to simulate a general irreversible Markov process on a closed manifold $\mathcal{N}$; see (1.4). In terms of the SDE, we will design a random walk approximation which enjoys ergodicity and accuracy. In terms of Fokker-Planck equation (1.2), we will design two upwind schemes with a Q-matrix[‡] structure so that they also enjoy ergodicity, unconditionally stability and accuracy.

[†]In some physics literature, it is referred as microscopic reversibility [28].

[‡]a.k.a. infinitesimal generator matrix for a Markov chain

Assume $\mathcal{N}$ is a d-dimensional closed manifold which is smooth enough. Let $\boldsymbol{b} \in T_{\mathcal{N}}$ be a given tangent vector field. We denote the over-damped Langevin dynamics of $\mathbf{y}$ by

$$\mathrm{d}\mathbf{y}_t = \boldsymbol{b}(\mathbf{y}_t)\,\mathrm{d}t + \sqrt{2}\sigma \sum_{i=1}^{d} \tau_i^{\mathcal{N}}(\mathbf{y}_t) \otimes \tau_i^{\mathcal{N}}(\mathbf{y}_t) \circ \mathrm{d}B_t, \tag{1.4}$$

where $\sigma \in \mathbb{R}^{\ell \times \ell}$ is a constant matrix corresponding to the thermal energy in physics, the symbol $\circ$ means the Stratonovich integral, B_t is ℓ-dimensional Brownian motion and $\{\tau_i^{\mathcal{N}}; 1 \le i \le d\}$ are orthonormal basis of tangent plane $T_{\mathbf{y}_t}\mathcal{N}$. Here $\nabla_{\mathcal{N}} := \sum_{i=1}^{d} \tau_i^{\mathcal{N}} \nabla_{\tau_i^{\mathcal{N}}} = \sum_{i=1}^{d} \tau_i^{\mathcal{N}} \otimes \tau_i^{\mathcal{N}} \nabla$ is the surface gradient and $\nabla_{\tau_i^{\mathcal{N}}} = \tau_i^{\mathcal{N}} \cdot \nabla$ is the tangential derivative in the direction of $\tau_i^{\mathcal{N}}$. More precise conditions on the manifold are described in [21, Chapter 4], [20]. By Ito's formula, the corresponding Fokker-Planck equation is

$$\partial_t \rho = -\nabla_{\mathcal{N}} \cdot (\boldsymbol{b}\rho) + \nabla_{\mathcal{N}} \cdot (D \nabla_{\mathcal{N}} \rho).$$

For simplicity of notation, we drop subscript $\mathcal{N}$ and still use (1.2).

In terms of a general Fokker-Planck equation on a closed manifold $\mathcal{N}$, if without detailed balance, we can decompose it as a gradient flow part (described by a symmetric operator) and a Hamiltonian flow part (described by an antisymmetric operator); see Section 2.2. It is important to design numerical schemes that preserves this structure in the discrete sense. Thus in Section 2, based on the Voronoi tessellation for manifold $\mathcal{N}$, we will develop two upwind finite volume schemes preserving stochastic Q-matrix structures and the discrete decompositions. The first upwind scheme does not rely on knowing the steady state π of irreversible dynamics (1.4); see Section 2.1. The second upwind scheme, which is called π-symmetric upwind scheme, leverages a given steady state information π to simulate irreversible dynamics (1.4) and also enjoys ergodicity to this given steady state; see Section 2.3. More importantly, schemes with stochastic Q-matrix structures always have a π-symmetric decomposition, which decomposes the discrete flux as a symmetric part (corresponding to a dissipation part) and an antisymmetric part (corresponding to an energy-conservative part); see Section 3. The later part has no contribution to the discrete energy dissipation, so we have same stability and ergodicity properties for both schemes; see Proposition 3.1 and Lemma 3.1. Moreover, based on the Q-matrix structure, we will propose an unconditionally stable implicit time discretization solved explicitly and prove its stability and exponential ergodicity; see Proposition 3.2.

In Section 4, we will give convergence and error estimates for the numerical steady state and the numerical dynamic solutions solved by the first upwind scheme (2.6), which rely on the Taylor expansion on the manifold and the discrete energy dissipation law; see Theorem 4.1. In Section 5, several numerical examples based on upwind scheme (2.6) and π-symmetric upwind scheme (2.27) are conducted: (i) accelerated sampling enhanced by an incompressible mixture flow; (ii) image transformations immersed in a mixture flow; and (iii) the stochastic Van der Pol oscillator in which we only know the drift vector field

$\boldsymbol{b}$ in the irreversible process. In the sampling and image examples, it is interesting to see the convection (the Hamiltonian flow part in the scheme) brought by the incompressible mixture flow speed up convergence of the dynamic solution to its steady state, which could be a promising direction to explore further in the future.

For Fokker-Planck equation (1.2) in a bounded open domain $\Omega \subset \mathbb{R}^\ell$ with various boundary conditions, there are many pioneering studies on numerical simulation. The most famous one is the Scharfetter-Gummel (SG) scheme proposed in [31] for some 1D semiconductor device equations; see Appendix B for detailed comparisons. Some extensions and mathematical analysis have been studied; e.g., [1, 25, 26, 35] and recently in [3]. We will follow similar ideas of a finite volume method for the drift-diffusion equation [2, 5, 10] but place more emphasis on the new Markov chain structures and π-symmetric decomposition. We develop the structure preserving schemes described above which possess stochastic Q-matrix structure and discrete π-symmetric decomposition. Particularly, our scheme also preserves irreversibility and recovers the original irreversible invariant measure. In summary, for our scheme (2.27), one has all the good properties including (i) positivity preserving; (ii) total mass preserving; (iii) well-balance property; (iv) ℓ^1-contraction; (v) the discrete π-symmetric decomposition (3.9); (vi) energy dissipation law; and (vii) ergodicity. Both of these schemes (2.6) and (2.27) naturally provide a random walk approximation for irreversible Markov processes on manifolds and thus also more easily adaptable to some data-driven algorithms based on high dimensional point clouds; c.f., [13, 18]. We also refer to [4] for exponential ergodicity of a hybrid finite volume schemes and refer to [32] for upwind schemes of aggregation–diffusion equations. The idea for the design of numerical schemes for these two recent work rooted in [32] but using a nonlinear approach which do not have Q-matrix properties.

The remaining paper will be organized as follows. In Section 2, we propose two upwind schemes with Q-matrix structure for the irreversible process (1.4). In Section 3, we give the discrete π-symmetric decomposition for a generic irreversible process on a closed manifold. Based on this, an energy dissipation law and exponential ergodicity are proved for both schemes. In Section 4, we give convergence and error estimates in terms of the χ^2-divergence. In Section 5, several numerical examples with/without steady state information are presented. Two schemes in the 2D structured grids case with no-flux boundary condition are given in appendix for completeness.

2 Two upwind schemes as random walk approximations for irreversible process

This section focuses on constructing random walk approximations for irreversible drift-diffusion process (1.4). The approximations are proposed based on some upwind finite volume schemes for the corresponding Fokker-Planck equation (1.2).

We focus on two kinds of fundamental problems in numerical simulations for irre-

versible process, i.e., the drift vector field $\boldsymbol{b}$ does not satisfy the detailed balance condition $\boldsymbol{b}=-D\nabla\phi$.

The first kind of problem is we only know the drift vector field $\boldsymbol{b}$ without steady state information. In this case, we will design an upwind scheme (2.6) with Q-matrix structure based on the Voronoi tessellation for manifold $\mathcal{N}$ to solve both numerical steady state and simulate the dynamic process described by (1.2); see Section 2.1.

The second kind of problem is that in many applications, we have information about the invariant measure π, although it is not detailed balanced (pointwise steady flux $F^{\pi}\neq 0$). This kinds of "steady state with nonzero flux on network" happens very common in biochemistry. In this case, we will design a π-symmetric upwind scheme (2.27) which recovers the given steady state π; see Section 2.3. This scheme is motivated by a reformulation as a gradient flow part and a Hamiltonian flow part for the continuous Fokker-Planck equation; see Section 2.2. Detailed analysis for upwind schemes with generic Q-matrix structure will be given in Section 3.

2.1 Voronoi tessellation and upwind finite volume scheme

In this section, we first propose a finite volume scheme for the Fokker-Planck equation (1.2) based on a Voronoi tessellation for $\mathcal{N}$. Then we design an upwind finite volume scheme with a Q-matrix structure, which can be reformulated as a Markov process on finite sites and enjoys good properties.

Suppose $(\mathcal{N},d_{\mathcal{N}})$ is a d dimensional smooth closed submanifold of $\mathbb{R}^{\ell}$ and $d_{\mathcal{N}}$ is induced by the Euclidean metric in $\mathbb{R}^{\ell}$. $S:=\{\mathbf{y}_i\}_{i=1:n}$ are point clouds sampled from a density function on $\mathcal{N}$ bounded below and above. It is proved that the data points S are well-distributed on $\mathcal{N}$ whenever the points are sampled from a density function with lower and upper bounds [33]. Using generating points $\{y_i\}$ and metric $d_{\mathcal{N}}$, define

$$C_i:=\{\mathbf{y}\in\mathcal{N};\ \mathrm{d}_{\mathcal{N}}(\mathbf{y},\mathbf{y}_i)\leq \mathrm{d}_{\mathcal{N}}(\mathbf{y},\mathbf{y}_j)\ \text{for all}\ \mathbf{y}_j\in S\}\quad \text{with volume}\ |C_i|=\mathcal{H}^d(C_i). \tag{2.1}$$

Here $\mathcal{H}^d(C_i)$ the d-dimensional Hausdorff measure of cell C_i. Then $\mathcal{N}=\cup_{i=1}^n C_i$ is a Voronoi tessellation of $\mathcal{N}$. Denote the Voronoi face for cell C_i as

$$\Gamma_{ij}:=C_i\cap C_j\quad \text{with its area}\ \ |\Gamma_{ij}|=\mathcal{H}^{d-1}(\Gamma_{ij}), \tag{2.2}$$

for any $j=1,\cdots,n$. If $\Gamma_{ij}=\emptyset$ or $i=j$ then we set $|\Gamma_{ij}|=0$. Define the associated adjacent sample points as

$$VF(i):=\{j;\ \Gamma_{ij}\neq\emptyset\}. \tag{2.3}$$

Using the above Voronoi tessellation, associated the discrete density $\rho_i|C_i|$ at cell C_i and the sign of the flux at each site, we design the upwind scheme as follows.

For each cell C_i, denote the unit outer normal vector field on ∂C_i (pointing from i to its adjacent j) as $\boldsymbol{n}\in\mathbb{R}^{\ell}$. Denote $(\boldsymbol{b}\cdot\boldsymbol{n})_{ij}^{+},(\boldsymbol{b}\cdot\boldsymbol{n})_{ij}^{-}>0$ as the positive and negative parts of $(\boldsymbol{b}\cdot\boldsymbol{n})_{ij}$ respectively, where $(\boldsymbol{b}\cdot\boldsymbol{n})_{ij}$ means evaluate $(\boldsymbol{b}\cdot\boldsymbol{n})$ at the intersection point of the

geodesic from $\mathbf{y}_i$ to $\mathbf{y}_j$. We integrate (1.2) on C_i and use the divergence theorem on cell C_i to obtain

$$\frac{\mathrm{d}}{\mathrm{d}t}\int_{C_i}\rho\mathcal{H}^d(C_i)=\sum_{j\in VF(i)}\int_{\Gamma_{ij}}\mathbf{n}\cdot(-\boldsymbol{b}\rho+D\nabla\rho)\mathcal{H}^{d-1}(\Gamma_{ij}). \tag{2.4}$$

The probability in C_i can be approximated as

$$\int_{C_i}\rho(\mathbf{y})\mathcal{H}^d(C_i)\approx\rho(\mathbf{y}_i)(1+\mathrm{diam}(C_i))|C_i|, \tag{2.5}$$

so we use ρ_i to approximate the exact solution $\rho(\mathbf{y}_i)$ on each cell C_i.

We introduce the following upwind finite volume scheme and call it "upwind scheme". For $i=1,\cdots,n$,

$$\frac{\mathrm{d}}{\mathrm{d}t}\rho_i|C_i|=\sum_{j\in VF(i)}|\Gamma_{ij}|\left(\frac{\boldsymbol{n}_{ij}\cdot D\boldsymbol{n}_{ij}\,(\rho_j-\rho_i)}{|\mathbf{y}_j-\mathbf{y}_i|}+(\boldsymbol{b}\cdot\boldsymbol{n})^-_{ij}\rho_j-(\boldsymbol{b}\cdot\boldsymbol{n})^+_{ij}\rho_i\right), \tag{2.6}$$

where $|C_i|$ is the volume element at cell C_i.

One can recast (2.6) as a matrix form

$$\frac{\mathrm{d}}{\mathrm{d}t}\rho_i|C_i|=\sum_j Q^*_{ij}\rho_j|C_j|,\quad i=1,\cdots,n, \tag{2.7}$$

where the Q^*-matrix is given by

$$Q^*_{ij}=\frac{|\Gamma_{ij}|}{|C_j|}\left(\frac{\boldsymbol{n}_{ij}\cdot D\boldsymbol{n}_{ij}}{|\mathbf{y}_j-\mathbf{y}_i|}+(\boldsymbol{b}\cdot n)^-_{ij}\right)\geq 0,\quad j\neq i,\quad Q^*_{ii}=\sum_{j\in VF(i)}\frac{|\Gamma_{ij}|}{|C_i|}\left(-\frac{\boldsymbol{n}_{ij}\cdot D\boldsymbol{n}_{ij}}{|\mathbf{y}_j-\mathbf{y}_i|}-(\boldsymbol{b}\cdot\boldsymbol{n})^+_{ij}\right). \tag{2.8}$$

Since for any two adjacent i and j, we have

$$\boldsymbol{n}_{ij}=-\boldsymbol{n}_{ji},\quad (\boldsymbol{b}\cdot\boldsymbol{n})^-_{ji}=(\boldsymbol{b}\cdot\boldsymbol{n})^+_{ij}. \tag{2.9}$$

Thus the transport of Q^* satisfies

$$\begin{aligned}&Q_{ij}=\frac{|\Gamma_{ij}|}{|C_i|}\left(\frac{\boldsymbol{n}_{ij}\cdot D\boldsymbol{n}_{ij}}{|\mathbf{y}_j-\mathbf{y}_i|}+(\boldsymbol{b}\cdot\boldsymbol{n})^-_{ji}\right)=\frac{|\Gamma_{ij}|}{|C_i|}\left(\frac{\boldsymbol{n}_{ij}\cdot D\boldsymbol{n}_{ij}}{|\mathbf{y}_j-\mathbf{y}_i|}+(\boldsymbol{b}\cdot\boldsymbol{n})^+_{ij}\right)\geq 0,\quad j\neq i,\\&Q_{ii}=-\sum_{j\in VF(i)}Q_{ij}.\end{aligned} \tag{2.10}$$

One can see Q-matrix is a stochastic matrix that row sums zero; see [23, Definition 2.3]. Then Q is the generator of the associated Markov process on point clouds. We list the following standard properties for Q-process (2.7), which guarantee good properties for the numerical scheme:

- positivity preserving, i.e., $\min_i\rho_i(0)\geq 0\Longrightarrow\min_i\rho_i(t)\geq 0$;

- total mass preserving, i.e., $\frac{\mathrm{d}}{\mathrm{d}t}\sum_i \rho_i|C_i| = \sum_{i,j} Q^*_{ij}\rho_j = 0$;
- ℓ^1-contraction, i.e., $\frac{\mathrm{d}}{\mathrm{d}t}\sum_i |\rho_i - \tilde{\rho}_i||C_i| \le \sum_{i,j} Q^*_{ij}|\rho_j - \tilde{\rho}_j| = 0$.

For the adjoint process $\partial_t f_i = \sum_j Q_{ij} f_j$, it satisfies maximal principle, i.e., for $i_m := \mathrm{argmin}_i f_i$ and $i_M := \mathrm{argmax}_i f_i$,

$$\frac{\mathrm{d}}{\mathrm{d}t} f_{i_m} = \sum_j Q_{i_m j}\left(f_j - f_{i_m}\right) \ge 0; \quad \frac{\mathrm{d}}{\mathrm{d}t} f_{i_M} = \sum_j Q_{i_M j}\left(f_j - f_{i_M}\right) \le 0.$$

When the exact metric for the manifold is unknown, we can also use collected point clouds which probe the manifold to compute an approximated Vonoroi tessellation; see details in [18, Algorithm 1]. We also give a comparison between our scheme and previous finite volume schemes in Appendix B.

Remark 2.1. One can interpret the upwind finite volume scheme (2.6) as the forward equation for a Markov process with transition probability P_{ji} (from j to i) and jump rate λ_j

$$\frac{\mathrm{d}}{\mathrm{d}t}\rho_i|C_i| = \sum_{j\in VF(i)} \lambda_j P_{ji}\rho_j|C_j| - \lambda_i\rho_i|C_i|, \quad i = 1,2,\cdots,n, \tag{2.11}$$

where for $i = 1,2,\cdots,n$,

$$\lambda_i := \sum_{j\neq i} Q_{ij}, \quad P_{ij} := \frac{Q_{ij}}{\lambda_i}, \quad j \in VF(i); \quad P_{ij} = 0, \quad j \notin VF(i). \tag{2.12}$$

Using the exponential distribution $f(t;\lambda) = \lambda e^{-\lambda t}$ with rate λ, one common construction of Q-process with generator Q is given by Gillespie's algorithm in the Monte Carlo simulation, i.e., given $X_t = i$, the probability for the event {after waiting time τ_i, the jump i to j, $X_{t+\tau} = j$ happens} is given by $P_{ij}\lambda_i e^{-\lambda_i\tau}$. This time-continuous Markov chain is an exact construction for the Q-process. There are also other time-discrete Markov chain constructions, which serve as good approximations for Q-process when time step $\Delta t \to 0$. For instance, let us assume (i) $X_t = i$, (ii) the probability for X_t stays at site i is $e^{-\lambda_i}\Delta t \approx 1 - \lambda_i\Delta t$, (iii) the probability for the jump i to j happens in $[t, t+\Delta t]$ is $\lambda_i\Delta t e^{-\lambda_i\Delta t} \approx \lambda_i\Delta t$. Then the corresponding master equation is just the forward Euler scheme for (2.11)

$$\rho_i^{k+1} = \rho_i^k(1 - \lambda_i\Delta t) + \sum_j \rho_j^k P_{ji}\lambda_j\Delta t. \tag{2.13}$$

The unconditionally stable explicit scheme (3.36) is another example for the time-discrete Markov chain construction of the Q-process.

Remark 2.2. The upwind finite volume scheme (2.6) belongs to monotone schemes uniform in D. It is well known all monotone schemes that uniform in D have at most first

order accuracy. To achieve higher order schemes for convection-dominated problems that enjoy the above positivity preserving property and still uniform in D, one need to restore some nonlinear schemes by the method of limiter or streamline diffusion methods. However, the nonlinearity will destroy the Q-matrix structure and we will leave high order schemes for a future study. On the other hand, in the case that diffusion D is not small, standard centered scheme can be adapted as a second order scheme.

2.2 Reformulate as gradient flow structure and Hamiltonian structure

Recall the continuous Fokker-Planck operator $\mathcal{L}^*$ in (1.2). From now on, to ensure existence of a positive invariant measure π, we assume D is positive definite. Based on [21, Proposition 4.5], we know the Fokker-Planck operator $\mathcal{L}^*$ on the compact manifold $\mathcal{N}$ has a unique invariant measure, denoted as π,

$$0=\mathcal{L}^*\pi=-\nabla\cdot(\boldsymbol{b}\pi)+\nabla\cdot(D\nabla\pi). \tag{2.14}$$

We first use the invariant measure π to decompose (1.2) as two parts: gradient flow part and Hamiltonian flow part. Rewrite (1.2) as

$$\begin{aligned}\partial_t\rho=&\mathcal{L}^*\rho=\nabla\cdot(D\nabla\rho-\boldsymbol{b}\rho)=\nabla\cdot\Big(D\pi\nabla\frac{\rho}{\pi}+\frac{\rho}{\pi}(D\nabla\pi-\pi\boldsymbol{b})\Big)\\ =&\nabla\cdot\Big(D\pi\nabla\frac{\rho}{\pi}\Big)+(D\nabla\pi-\pi\boldsymbol{b})\cdot\nabla\frac{\rho}{\pi}=:L^*\frac{\rho}{\pi}+T\frac{\rho}{\pi}.\end{aligned} \tag{2.15}$$

Here the symmetric operator L^* is

$$L^*:=\nabla\cdot(D\pi\nabla),\quad \text{with}\ \ \langle f,L^*g\rangle=\langle L^*f,g\rangle,\quad \langle u,L^*u\rangle\le 0, \tag{2.16}$$

while the antisymmetric operator T is

$$T:=(D\nabla\pi-\pi\boldsymbol{b})\cdot\nabla=:\boldsymbol{u}\cdot\nabla,\quad \text{with}\ \ \langle f,Tg\rangle=-\langle Tf,g\rangle \tag{2.17}$$

since $\nabla\cdot(D\nabla\pi-\pi\boldsymbol{b})=\nabla\cdot\boldsymbol{u}=0$ by (2.14). Here we remark that in terms of ρ-variable, we usually say $\nabla\cdot\big(D\pi\nabla\frac{1}{\pi}\big)$ (resp. $\boldsymbol{u}\cdot\nabla\frac{1}{\pi}$) is symmetric (resp. antisymmetric) operator in $L^2(\frac{1}{\pi})$. We will call this decomposition as 'π-symmetric decomposition'.

In the irreversible case, (2.15) for the reformulated Fokker-Planck equation can be regarded as a gradient flow part $\partial_t\rho=L^*\frac{\rho}{\pi}=\nabla\cdot\big(D\pi\nabla\frac{\rho}{\pi}\big)$ plus a Hamiltonian flow part (convection part) $\partial_t\rho=T\frac{\rho}{\pi}=(D\nabla\pi-\pi\boldsymbol{b})\cdot\nabla\frac{\rho}{\pi}$. Indeed, given a convex function ϕ with $\phi''\ge 0$, denote the free energy as

$$E:=\int\phi\Big(\frac{\rho}{\pi}\Big)\pi\mathrm{d}x. \tag{2.18}$$

Since $\nabla\cdot(D\nabla\pi-\pi\boldsymbol{b})=0$, for any free energy of the form (2.18), we have

$$\Big\langle\frac{\delta E}{\delta\rho},T\frac{\rho}{\pi}\Big\rangle=\Big\langle\phi'\Big(\frac{\rho}{\pi}\Big),T\frac{\rho}{\pi}\Big\rangle=\int(D\nabla\pi-\pi\boldsymbol{b})\cdot\nabla\phi\Big(\frac{\rho}{\pi}\Big)\,\mathrm{d}x=0. \tag{2.19}$$

For the gradient flow part, we have

$$\left\langle \frac{\delta E}{\delta \rho}, L^* \frac{\rho}{\pi} \right\rangle = \left\langle \phi'\left(\frac{\rho}{\pi}\right), L^* \frac{\rho}{\pi} \right\rangle = -\int \phi''\left(\frac{\rho}{\pi}\right) \pi \nabla \frac{\rho}{\pi} \cdot D \nabla \frac{\rho}{\pi} \mathrm{d}x \leq 0. \tag{2.20}$$

This observation is quite similar to the so called GENERIC (general equation for non-equilibrium reversible-irreversible coupling) formalism, which also decomposes a general thermodynamics as a gradient flow part and a Hamiltonian flow part.

From (2.19), in terms of the energy dissipation law, the Hamiltonian part has no contribution. From now on, we denote c as a generic constant whose value may change from line to line.

Below we summarize the following lemma for the energy dissipation law for continuous equation and later we will use it to derive a corresponding discrete energy dissipation law.

Lemma 2.1. *Let E be an entropy defined in* (2.18)*, we have the energy dissipation law*

$$\frac{\mathrm{d}E}{\mathrm{d}t} = -\int \phi''\left(\frac{\rho}{\pi}\right) \pi \nabla \frac{\rho}{\pi} \cdot D \nabla \frac{\rho}{\pi} \mathrm{d}x \leq 0. \tag{2.21}$$

Specially, it is well known that the reversible condition (detailed balance condition) is equivalent to $\boldsymbol{b} = D\nabla \log \pi$, i.e., there is only symmetric part $\partial_t \rho = L^* \frac{\rho}{\pi}$. In this case, there are particularly two well known gradient flow structures:

(i) Take $\phi(x) = x \log x$ then free energy becomes $\mathrm{KL}(\rho||\pi) = \int \rho \log \frac{\rho}{\pi} \mathrm{d}x$, and we have the gradient flow

$$\partial_t \rho = \nabla \cdot \left(\rho D \nabla \frac{\delta \mathrm{KL}}{\delta \rho} \right); \quad \frac{\mathrm{d}}{\mathrm{d}t} \mathrm{KL}(\rho||\pi) = -\left\langle \rho \nabla \log \frac{\rho}{\pi}, D \nabla \log \frac{\rho}{\pi} \right\rangle \leq 0; \tag{2.22}$$

(ii) Take $\phi(x) = \frac{1}{2}x^2$, then free energy becomes χ^2-divergence $\chi^2(\rho) = \frac{1}{2}\int \frac{\rho^2}{\pi} \mathrm{d}x$, and we have the gradient flow

$$\partial_t \rho = \nabla \cdot \left(\pi D \nabla \frac{\delta \chi^2(\rho)}{\delta \rho} \right); \quad \frac{\mathrm{d}}{\mathrm{d}t} \chi^2(\rho) = -\left\langle \pi \nabla \frac{\rho}{\pi}, D \nabla \frac{\rho}{\pi} \right\rangle \leq 0. \tag{2.23}$$

Particularly, take $\phi(x) = \frac{1}{2}(x-1)^2$, then we have the decay estimate for $\frac{1}{2}\int \frac{(\rho-\pi)^2}{\pi} \mathrm{d}x$,

$$\frac{\mathrm{d}}{\mathrm{d}t} \frac{1}{2} \int \frac{(\rho-\pi)^2}{\pi} \mathrm{d}x = -\left\langle \pi \nabla \frac{\rho}{\pi}, D \nabla \frac{\rho}{\pi} \right\rangle \leq 0. \tag{2.24}$$

This together with Poincare's inequality

$$\int |u|^2 \pi \mathrm{d}x \leq c \langle \pi \nabla u, D \nabla u \rangle \quad \text{for } \int u \pi \mathrm{d}x = 0,$$

yields the exponential decay of ρ to steady state π.

Thanks to Poincare's inequality, π-symmetric decomposition (2.15) and Lemma 2.1, we conclude that in terms of exponential ergodicity, there is no difference between the irreversible process and the corresponding reversible process. Indeed, the equivalence of the exponential ergodicity for the irreversible process and the corresponding reversible process was already established in [6]; particularly for countable state space. Moreover, besides the gradient flow part, the incompressible transport $\boldsymbol{u}\cdot\nabla\frac{\rho}{\pi}$ brought by $\boldsymbol{u}=D\nabla\pi-\pi\boldsymbol{b}$ usually results in mixture. Thus we will observe a speedup of convergence for the irreversible process; see Section 5.1.

From π-symmetric decomposition (2.15), for the irreversible case, the dynamics can not be described only by a gradient flow and there is an additional Hamiltonian flow part. This observation is also given by [27, Example 4.3]. Moreover, by defining a L-function in the large deviation principle, [12, 27] established the relation between (generalized) gradient flow and the L-function in the large deviation principle; see also [14, 15, 17].

Designing a structure preserving numerical scheme is important and will be studied for schemes with generic Q-matrix structure in Section 3 via a discrete π-symmetric decomposition. Specifically, we will show both "upwind scheme" (2.6) and "π-symmetric upwind scheme" (2.27) are structure preserving numerical scheme which enjoy the above π-symmetric decomposition, a discrete dissipation law and exponential ergodicity.

2.3 π-symmetric upwind scheme for irreversible processes with an invariant measure

In this section, we design a finite volume scheme based on π-symmetric decomposition (2.15) and based on a given steady state information, i.e., the invariant measure π. The expected numerical scheme, which defines a numerical π_i^∞, should recover the given steady state $\pi_i^\infty=\pi_i$. This kind of idea that preserves given steady state is known as "well-balanced scheme." Recall the symmetric decomposition (2.15)

$$\partial_t\rho=\nabla\cdot(D\nabla\rho-\boldsymbol{b}\rho)=\nabla\cdot\left(D\pi\nabla\frac{\rho}{\pi}\right)+(D\nabla\pi-\pi\boldsymbol{b})\cdot\nabla\frac{\rho}{\pi}=:L^*\frac{\rho}{\pi}+T\frac{\rho}{\pi}. \tag{2.25}$$

From stationary equation (2.14), the new drift velocity

$$\boldsymbol{u}:=D\nabla\pi-\pi\boldsymbol{b},\quad \nabla\cdot\boldsymbol{u}=0. \tag{2.26}$$

Then two common scenarios in applications are (i) given the non-gradient form drift $\boldsymbol{b}$ and steady state π, we can compute the new drift velocity (2.26); (ii) given any incompressible velocity field $\boldsymbol{u}$ such that $\nabla\cdot\boldsymbol{u}=0$, based on π, then the original drift is given by $\boldsymbol{b}=D\frac{\nabla\pi}{\pi}+\frac{\boldsymbol{u}}{\pi}$.

Now using the symmetric decomposition (2.15) and the given steady state information π, we design the following upwind finite volume scheme and call it "π-symmetric upwind scheme". For $i=1,\cdots,n$,

$$\frac{\mathrm{d}}{\mathrm{d}t}\rho_i|C_i|=\sum_{j\in VF(i)}|\Gamma_{ij}|\left(\frac{D(\pi_i+\pi_j)}{2|\mathbf{y}_j-\mathbf{y}_i|}\left(\frac{\rho_j}{\pi_j}-\frac{\rho_i}{\pi_i}\right)+(\boldsymbol{u}\cdot\boldsymbol{n})_{ij}^-\frac{\rho_j}{\pi_j}-(\boldsymbol{u}\cdot\boldsymbol{n})_{ij}^+\frac{\rho_i}{\pi_i}\right), \tag{2.27}$$

where $|C_i|$ is the volume element at cell C_i. Here $(\boldsymbol{u}\cdot\boldsymbol{n})_{ij}^+, (\boldsymbol{u}\cdot\boldsymbol{n})_{ij}^- > 0$ as the positive and negative parts of $(\boldsymbol{u}\cdot\boldsymbol{n})_{ij}$ respectively.

Denote

$$\begin{aligned} Q_{ij}^* &= \frac{|\Gamma_{ij}|}{|\pi_j||C_j|}\left(\frac{D(\pi_i+\pi_j)}{2|\mathbf{y}_j-\mathbf{y}_i|}+(\boldsymbol{u}\cdot\boldsymbol{n})_{ij}^-\right)\geq 0, \quad j\neq i, \\ Q_{ii}^* &= \sum_j \frac{|\Gamma_{ij}|}{|\pi_i||C_i|}\left(-\frac{D(\pi_i+\pi_j)}{2|\mathbf{y}_j-\mathbf{y}_i|}-(\boldsymbol{u}\cdot\boldsymbol{n})_{ij}^+\right). \end{aligned} \tag{2.28}$$

Then from (2.9)

$$Q_{ij}^* = Q_{ji} = \frac{|\Gamma_{ij}|}{|\pi_j||C_j|}\left(\frac{D(\pi_i+\pi_j)}{2|\mathbf{y}_j-\mathbf{y}_i|}+(\boldsymbol{u}\cdot\boldsymbol{n})_{ij}^-\right)\geq 0, \quad j\neq i, \quad Q_{ii} = -\sum_{j\neq i} Q_{ij}, \tag{2.29}$$

which is still a stochastic Q-matrix that row sums zero. Then (2.27) can be recast as

$$\frac{\mathrm{d}}{\mathrm{d}t}\rho_i|C_i| = \sum_j Q_{ij}^*\rho_j|C_j|. \tag{2.30}$$

2.3.1 Structure preserving decomposition

For the upwind part of (2.27), notice

$$(\boldsymbol{u}\cdot\boldsymbol{n})_{ij}^+\frac{\rho_j}{\pi_j} = (\boldsymbol{u}\cdot\boldsymbol{n})_{ij}\frac{\rho_i}{\pi_i} + (\boldsymbol{u}\cdot\boldsymbol{n})_{ij}^-\frac{\rho_i}{\pi_i}. \tag{2.31}$$

Then the flux F_{ji} in (2.27) can be recast as

$$F_{ji} = |\Gamma_{ij}|\left(\left(\frac{D(\pi_i+\pi_j)}{2|\mathbf{y}_j-\mathbf{y}_i|}+(\boldsymbol{u}\cdot\boldsymbol{n})_{ij}^-\right)\left(\frac{\rho_j}{\pi_j}-\frac{\rho_i}{\pi_i}\right)-(\boldsymbol{u}\cdot\boldsymbol{n})_{ij}\frac{\rho_i}{\pi_i}\right). \tag{2.32}$$

Notice another anti-symmetric decomposition for the upwind parts

$$(\boldsymbol{u}\cdot\boldsymbol{n})_{ij}^-\frac{\rho_j}{\pi_j}-(\boldsymbol{u}\cdot\boldsymbol{n})_{ij}^+\frac{\rho_i}{\pi_i} = -\frac{1}{2}(\boldsymbol{u}\cdot\boldsymbol{n})_{ij}\left(\frac{\rho_j}{\pi_j}+\frac{\rho_i}{\pi_i}\right)+\frac{1}{2}|(\boldsymbol{u}\cdot\boldsymbol{n})_{ij}|\left(\frac{\rho_j}{\pi_j}-\frac{\rho_i}{\pi_i}\right). \tag{2.33}$$

Then another recast of flux F_{ji} in (2.27) is

$$F_{ji} = |\Gamma_{ij}|\left(\left(\frac{D(\pi_i+\pi_j)}{2|\mathbf{y}_j-\mathbf{y}_i|}+\frac{1}{2}|(\boldsymbol{u}\cdot\boldsymbol{n})_{ij}|\right)\left(\frac{\rho_j}{\pi_j}-\frac{\rho_i}{\pi_i}\right)-\frac{1}{2}(\boldsymbol{u}\cdot\boldsymbol{n})_{ij}\left(\frac{\rho_j}{\pi_j}+\frac{\rho_i}{\pi_i}\right)\right). \tag{2.34}$$

Using (2.34), multiplying (2.27) by $\frac{\rho_i}{\pi_i}$ and taking summation w.r.t i, we have

$$\begin{aligned} \frac{\mathrm{d}}{\mathrm{d}t}\frac{\rho_i^2}{\pi_i}|C_i| &= -\sum_{i,j}\frac{|\Gamma_{ij}|}{2}\left(\frac{D(\pi_i+\pi_j)}{|\mathbf{y}_j-\mathbf{y}_i|}+|(\boldsymbol{u}\cdot\boldsymbol{n})_{ij}|\right)\left(\frac{\rho_j}{\pi_j}-\frac{\rho_i}{\pi_i}\right)^2+I_e, \\ I_e &:= -\sum_{i,j}\frac{|\Gamma_{ij}|}{2}(\boldsymbol{u}\cdot\boldsymbol{n})_{ij}\left(\frac{\rho_j}{\pi_j}\frac{\rho_i}{\pi_i}+\frac{\rho_i^2}{\pi_i^2}\right) = -\sum_{i,j}\frac{|\Gamma_{ij}|}{2}(\boldsymbol{u}\cdot\boldsymbol{n})_{ij}\frac{\rho_i^2}{\pi_i^2}. \end{aligned} \tag{2.35}$$

Notice in the continuous case, given π and $\boldsymbol{b}$, the drift $\boldsymbol{u}$ in (2.26) is divergence free. If we have same divergence free condition in the discrete case, then $I_e=0$ and we obtain the accurate convergence to steady state. Thus we construct the discrete velocity field such that the incompressible condition holds

$$\sum_j |\Gamma_{i,j}|(\boldsymbol{u}\cdot\boldsymbol{n})_{i,j}=0. \tag{2.36}$$

There are some well-known schemes in computations for incompressible flows, Maxwell's equations and magnetohydrodynamics [9,24]. We adapt them in the 2D case as follows. In 2D, there exists a stream function $\psi(x,y)$ such that $\boldsymbol{u}=(-\partial_y\psi,\partial_x\psi)$. For each 2D cell C_i, we set a counterclockwise orientation for its face $\Gamma_{ij}, j\in VF(i)$. Then at each face Γ_{ij}, denote the starting point as α_{ij} and the ending point as β_{ij}. Then the discrete incompressible velocity field is defined as

$$(\boldsymbol{u}\cdot\boldsymbol{n})_{ij}:=\partial_\tau\psi\approx\frac{\psi(\beta_{ij})-\psi(\alpha_{ij})}{|\beta_{ij}-\alpha_{ij}|}=\frac{\psi(\beta_{ij})-\psi(\alpha_{ij})}{|\Gamma_{ij}|}, \tag{2.37}$$

which automatically satisfies (2.36). In 3D case, we need use a vector potential instead of stream function while in higher dimension there are more freedoms to construct the incompressible velocity.

Thanks to (2.36) and $I_e=0$, (2.35) becomes the discrete energy dissipation law

$$\frac{\mathrm{d}}{\mathrm{d}t}\frac{\rho_i^2}{\pi_i}|C_i|=-\frac{1}{2}\sum_{i,j}\alpha_{i,j}\left(\frac{\rho_j}{\pi_j}-\frac{\rho_i}{\pi_i}\right)^2\leq 0 \tag{2.38}$$

with a symmetric coefficient $\alpha_{ij}=|\Gamma_{ij}|\big(\frac{D(\pi_i+\pi_j)}{|\mathbf{y}_j-\mathbf{y}_i|}+|(\boldsymbol{u}\cdot\boldsymbol{n})_{ij}|\big)$; see Proposition 3.1 for same result with a general Q-matrix. Then with the truncation error estimate, we will give the convergence analysis in Theorem 4.1 for the numerical solution in terms of the χ^2-divergence.

After choosing $\boldsymbol{u}$ satisfying (2.36), from (2.32), π-symmetric upwind scheme (2.27) is equivalent to

$$\frac{\mathrm{d}}{\mathrm{d}t}\rho_i|C_i|=\sum_{j\in VF(i)}F_{ji},\quad F_{ji}=|\Gamma_{ij}|\left(\frac{D(\pi_i+\pi_j)}{2|\mathbf{y}_j-\mathbf{y}_i|}+(\boldsymbol{u}\cdot\boldsymbol{n})_{ij}^-\right)\left(\frac{\rho_j}{\pi_j}-\frac{\rho_i}{\pi_i}\right). \tag{2.39}$$

Thus although the original Fokker-Planck (1.2) is irreversible, but the discrete flux F_{ji} can be chosen such that the discrete steady flux

$$F_{ji}^{\pi}=|\Gamma_{ij}|\left(\frac{D(\pi_i+\pi_j)}{2|\mathbf{y}_j-\mathbf{y}_i|}+(\boldsymbol{u}\cdot\boldsymbol{n})_{ij}^-\right)\left(\frac{\pi_j}{\pi_j}-\frac{\pi_i}{\pi_i}\right)\equiv 0,\quad \forall i,j. \tag{2.40}$$

This implies the scheme is well balanced, i.e., numerical steady state $\pi_i^\infty=\pi_i$.

Remark 2.3. Although we can choose the discrete flux satisfies (2.40), we remark this does not contradict with the equivalent irreversible condition, i.e., the flux $F^\pi = 0$ pointwisely for continuous Fokker-Planck equation; c.f. [15, 30]. Indeed, because of different decomposition of flux and (2.36), in the numerical schemes, one can either use the pointwise flux F_{ji} in (2.39) or use original F_{ji} in (2.32); however, only the former one satisfies (2.40).

Remark 2.4. Although we design numerical schemes under the assumption $\mathcal{N}$ is a closed manifold, for manifold with boundaries, we point out the construction of schemes and the analysis for no-flux boundary condition are identically same because $j \in VF(i)$ in both schemes (2.6) and (2.27) already accommodate the no-flux boundary conditions for i adjacent to the boundary. In the numerical examples in Section 5, for 2D structured grids, schemes (2.6) and (2.27) naturally equip with no-flux boundary conditions.

3 Structure preserving, ergodicity and stability

In this section, for numerical schemes with an abstract generic Q-matrix structure, we present a structure preserving reformulation, which is the discrete counterpart of π-symmetric decomposition (2.15). Then we use it to prove stability and ergodicity for schemes with a generic Q-matrix structure. These results apply to both (2.6) and (2.27).

3.1 Structure preserving for the π-symmetric decomposition in discrete case

In this section, we leverage the numerical steady state π_i^∞ to recover the π-symmetric decomposition for numerical schemes with a generic Q-matrix structure, for instance (2.6), and derive the discrete energy dissipation law. We will show that all the structures for continuous equation are also preserved for our numerical scheme including (i) positivity preserving; (ii) total mass preserving; (iii) well-balance property; (iv) ℓ^1-contraction; (v) the discrete π-symmetric decomposition (3.9); and (vi) energy dissipation law.

Step 1. As we already observed in (2.29), Q defined in (2.29) is a stochastic Q-matrix. Thus (i) positivity preserving and (ii) the total mass preserving are straightforward. The well-balanced property directly comes from (2.40). For (iv), one can see for any ρ_i and $\tilde{\rho}_i$ and $e_i = \rho_i - \tilde{\rho}_i$

$$\frac{\mathrm{d}}{\mathrm{d}t}\sum_i |e_i| = \sum_{i,j} Q_{ji}\mathrm{sgn}(e_i)e_j \le \sum_{i,j} Q_{ji}|e_j| = 0, \tag{3.1}$$

due to $\sum_j Q_{ij} = 0$. Thus (iv) ℓ^1-contraction holds.

Step 2. Before doing the symmetric decomposition, we first clarify the existence and uniqueness of a positive numerical steady state π^∞. Since our scheme is well-balanced (2.40), the numerical steady state $\pi^\infty = \pi$ exists. Next, we show the uniqueness of π^∞ using the Perron-Frobenius theorem. Let Q be the Q-matrix defined in (2.10). Notice the

Vonoroi tessellation implies the directed graph associated to Q is connected. Thus Q is irreducible. Taking a constant $a>\max_i(-Q_{ii})>0$, we construct a transition probability matrix

$$K:=\frac{Q}{a}+I \tag{3.2}$$

such that

$$K_{ij}=\frac{Q_{ij}}{a}\geq 0,\quad j\neq i;\quad K_{ii}=1+\frac{Q_{ii}}{a}>0. \tag{3.3}$$

Since $K_{ii}>0$, the resulted Markov chain with transition probability matrix K is aperiodic. It is easy to see $\sum_j K_{ij}=1$, so we know 1 is an eigenvalue to K with a right eigenvector $e:=(1,1,\cdots,1)^T$, i.e. $Ke=e$. Then by the Perron-Frobenius theorem for K, we know

- $\mu_1=1$ is the principle eigenvalue of K and all the other eigenvalues $|\mu_i|<1$, $i=2,\cdots,n$;
- there is a positive eigenvector, denoted as π_∞^T, being the left eigenvector corresponding to 1, i.e. $\pi_\infty^T K=\pi_\infty^T$.

Here and in the following context, the vector ρ^T is short for $\rho^T:=(\rho_1|C_1|,\cdots,\rho_n|C_n|)$. Thus we know the positive vector π^∞ is the unique numerical stationary solution to

$$\sum_j Q_{ij}^*\pi_j^\infty|C_j|=0. \tag{3.4}$$

One can interpret the right-hand-side of (2.7) as the flux gained and lost at site i. Denote

$$F_{ji}:=Q_{ji}\rho_j|C_j|-Q_{ij}\rho_i|C_i|, \tag{3.5}$$

then the dynamic solution satisfies

$$\partial_t(\rho_i|C_i|)=\sum_{j\in VF(i)}F_{ji},\quad i=1,2,\cdots,n. \tag{3.6}$$

Denote the steady flux as

$$F_{ji}^\pi:=Q_{ji}\pi_j^\infty|C_j|-Q_{ij}\pi_i^\infty|C_i|,\quad \sum_{j\in VF(i)}F_{ji}^\pi=0 \tag{3.7}$$

then we have the symmetric property

$$F_{ij}=-F_{ji},\quad F_{ij}^\pi=-F_{ji}^\pi. \tag{3.8}$$

Next, leveraging the positive numerical steady state π^∞, we reformulate the flux F_{ji} using a discrete π-symmetric decomposition. Using an elementary identity, we have

$$\begin{aligned}
F_{ji}=&Q_{ji}\rho_j|C_j|-Q_{ij}\rho_i|C_i|\\
=&\frac{Q_{ji}\pi_j^\infty|C_j|+Q_{ij}\pi_i^\infty|C_i|}{2}\left(\frac{\rho_j}{\pi_j^\infty}-\frac{\rho_i}{\pi_i^\infty}\right)+\frac{Q_{ji}\pi_j^\infty|C_j|-Q_{ij}\pi_i^\infty|C_i|}{2}\left(\frac{\rho_j}{\pi_j^\infty}+\frac{\rho_i}{\pi_i^\infty}\right)\\
=&\frac{1}{2}\alpha_{ij}\left(\frac{\rho_j}{\pi_j^\infty}-\frac{\rho_i}{\pi_i^\infty}\right)+\frac{1}{2}F_{ji}^\pi\left(\frac{\rho_j}{\pi_j^\infty}+\frac{\rho_i}{\pi_i^\infty}\right)=:L_{ij}+T_{ij},
\end{aligned} \tag{3.9}$$

where $\alpha_{ij} := Q_{ji}\pi_j^\infty|C_j| + Q_{ij}\pi_i^\infty|C_i| = \alpha_{ji} > 0$ is the symmetric positive coefficients. For the reversible case, α_{ij} is known as Onsager matrix.

From the row sums zero property for Q-matrix, the natural tangent space of the probability space will be $T_P := \{u \in \mathbb{R}^n;\ \sum_i u_i = 0 \text{ and } u_i \geq 0 \text{ if } \rho_i = 0\}$. Then from the antisymmetric property, we have

$$\sum_{ij} \alpha_{ij}\left(\frac{\rho_j}{\pi_j^\infty} - \frac{\rho_i}{\pi_i^\infty}\right) = 0, \quad \sum_{ij} F_{ji}^\pi \left(\frac{\rho_j}{\pi_j^\infty} + \frac{\rho_i}{\pi_i^\infty}\right) = 0. \tag{3.10}$$

Thus (v) discrete π-symmetric decomposition (3.9) holds. It ensures each component in the decomposition still belongs to the tangent space T_P.

From stationary equation (3.7) and (2.9), we have

$$\sum_j T_{ij} = \sum_j \frac{F_{ji}^\pi}{2}\frac{\rho_j}{\pi_j^\infty}, \quad \sum_{i,j} T_{ij}\frac{\rho_i}{\pi_i^\infty} = \sum_{i,j} F_{ji}^\pi \frac{\rho_j}{\pi_j^\infty}\frac{\rho_i}{\pi_i^\infty} = 0. \tag{3.11}$$

Therefore the second part T_{ij} in the decomposition has no contribution in the energy dissipation law. Indeed, if the reversible condition (detailed balance) holds, i.e., $Q_{ji}\pi_j^\infty|C_j| = Q_{ij}\pi_i^\infty|C_i|$, then $T_{ij} = 0$ and we obtain exactly same energy dissipation law as the irreversible case. However, for the irreversible case, i.e., $Q_{ji}\pi_j^\infty|C_j| \neq Q_{ij}\pi_i^\infty|C_i|$, PRIGOGINE characterized the energy transport when the dynamical system reaches the "stationary non-equilibrium state π" via the concept of entropy production rate [29]. Irreversible process is important for computing transition paths in chemical reaction [13] and constructing the global energy landscape [16]. Importantly, using Markov chain models in biochemical reactions, HILL gives the following specific formula for the entropy production rate and call it "the total rate of free energy dissipation" [19, eq. (9.20)]

$$\mathrm{d}S := \frac{kT}{2}\sum_{i,j}\left(Q_{ij}\pi_i^\infty|C_i| - Q_{ji}\pi_j^\infty|C_j|\right)\log\frac{Q_{ij}\pi_i^\infty|C_i|}{Q_{ji}\pi_j^\infty|C_j|} > 0. \tag{3.12}$$

Apparently, $\mathrm{d}S = 0$ if and only if the detailed balance condition holds (reversible case). See Appendix C for detailed derivations by HILL.

In the following convergence analysis, since D is positive definite, so $\boldsymbol{n}_{ij}\cdot D\boldsymbol{n}_{ij} \geq c > 0$. Thus for notation simplicity, we now assume $D_{ij} = D\delta_{ij}, D > 0$ is a scalar constant. From the definition of Q for (2.6),

$$F_{ji} = |\Gamma_{ij}|\left(\frac{D(\rho_j - \rho_i)}{|\mathbf{y}_j - \mathbf{y}_i|} + (\boldsymbol{b}\cdot\boldsymbol{n})_{ij}^-\rho_j - (\boldsymbol{b}\cdot\boldsymbol{n})_{ij}^+\rho_i\right).$$

Respectively, the steady flux at site i is

$$F_{ji}^\pi = |\Gamma_{ij}|\left(\frac{D\left(\pi_j^\infty - \pi_i^\infty\right)}{|\mathbf{y}_j - \mathbf{y}_i|} + (\boldsymbol{b}\cdot\boldsymbol{n})_{ij}^-\pi_j^\infty - (\boldsymbol{b}\cdot\boldsymbol{n})_{ij}^+\pi_i^\infty\right). \tag{3.13}$$

We summarize (vi) discrete energy dissipation law below.

Proposition 3.1. Let ρ_i be the solution to (3.6) and π_i^∞ be the solution to (3.7).

$$\begin{aligned}\frac{\mathrm{d}}{\mathrm{d}t}\sum_i \frac{\rho_i^2}{\pi_i^\infty}|C_i| &= -\frac{1}{2}\sum_{i,j}\alpha_{ij}\left(\frac{\rho_j}{\pi_j^\infty}-\frac{\rho_i}{\pi_i^\infty}\right)^2 \\ &\leq -\frac{D}{2}\sum_{i,j}\frac{|\Gamma_{ij}|(\pi_i^\infty+\pi_j^\infty)}{|\mathbf{y}_i-\mathbf{y}_j|}\left(\frac{\rho_j}{\pi_j^\infty}-\frac{\rho_i}{\pi_i^\infty}\right)^2 \leq 0, \end{aligned} \tag{3.14}$$

where $\alpha_{ij}=Q_{ji}\pi_j^\infty|C_j|+Q_{ij}\pi_i^\infty|C_i|=\alpha_{ji}>0$. Moreover, we have also

$$\begin{aligned}\frac{\mathrm{d}}{\mathrm{d}t}\sum_i \frac{(\rho_i-\pi_i^\infty)^2}{\pi_i^\infty}|C_i| &= -\frac{1}{2}\sum_{i,j}\alpha_{ij}\left(\frac{\rho_j}{\pi_j^\infty}-\frac{\rho_i}{\pi_i^\infty}\right)^2 \\ &\leq -\frac{D}{2}\sum_{i,j}\frac{|\Gamma_{ij}|(\pi_i^\infty+\pi_j^\infty)}{|\mathbf{y}_i-\mathbf{y}_j|}\left(\frac{\rho_j}{\pi_j^\infty}-\frac{\rho_i}{\pi_i^\infty}\right)^2 \leq 0. \end{aligned} \tag{3.15}$$

We remark the χ^2-divergence energy identity (3.14) always holds with/without detailed balance condition. Usually the dissipation term $\frac{1}{2}\sum_{i,j}\alpha_{ij}\left(\frac{\rho_j}{\pi_j^\infty}-\frac{\rho_i}{\pi_i^\infty}\right)^2$ is called discrete Dirichlet form. As a consequence, the symmetric coefficients for "upwind scheme" is

$$\alpha_{ij}:=|\Gamma_{ij}|\left(\frac{D}{|\mathbf{y}_j-\mathbf{y}_i|}\left(\pi_i^\infty+\pi_j^\infty\right)+(\boldsymbol{b}\cdot\boldsymbol{n})_{ij}^+\pi_i^\infty+(\boldsymbol{b}\cdot\boldsymbol{n})_{ji}^+\pi_j^\infty\right)=\alpha_{ji}, \tag{3.16}$$

while for "π-symmetric upwind scheme" is

$$\alpha_{ij}=|\Gamma_{ij}|\left(\frac{D(\pi_i+\pi_j)}{|\mathbf{y}_j-\mathbf{y}_i|}+|(\boldsymbol{u}\cdot\boldsymbol{n})_{ij}|\right)=\alpha_{ji}. \tag{3.17}$$

Proof. Using the definition of Q, direct calculations show $\alpha_{ij}=Q_{ji}\pi_j^\infty|C_j|+Q_{ij}\pi_i^\infty|C_i|$ is given by (3.16). From the decomposition (3.9) and (3.11), the discrete energy dissipation law becomes

$$\sum_i \frac{\rho_i}{\pi_i^\infty}\dot{\rho}_i|C_i|=\sum_i\left(\frac{\rho_i}{\pi_i^\infty}\sum_j F_{ji}\right)=-\frac{1}{4}\sum_{i,j}\alpha_{ij}\left(\frac{\rho_j}{\pi_j^\infty}-\frac{\rho_i}{\pi_i^\infty}\right)^2\leq 0. \tag{3.18}$$

Since π^∞ is positive, we have the estimate

$$\alpha_{ij}>D\frac{|\Gamma_{ij}|(\pi_i^\infty+\pi_j^\infty)}{|\mathbf{y}_j-\mathbf{y}_i|}. \tag{3.19}$$

Then (3.18) implies (3.14). Moreover, from conservation of total mass,

$$\sum_i \frac{\rho_i}{\pi_i^\infty}\dot{\rho}_i|C_i|=\sum_i\left(\frac{\rho_i}{\pi_i^\infty}-1\right)\dot{\rho}_i|C_i|=\frac{1}{2}\frac{\mathrm{d}}{\mathrm{d}t}\sum_i\frac{(\rho_i-\pi_i^\infty)^2}{\pi_i^\infty}|C_i|, \tag{3.20}$$

so we also conclude (3.15). □

We point out that the stability analysis here and in the remaining section also works for the Fokker-Planck equation on non-compact manifold as long as a positive solution to $Q^*\pi^\infty=0$ exists. However, there is no general Perron-Frobenius theorem to ensure the existence of (3.4) for a Q-matrix on a countable states.

Remark 3.1. Compared with the π-symmetric decomposition in the continuous case (2.15), the gradient flow part in (3.9)

$$L_{ij}=\frac{D|\Gamma_{ij}|}{|\mathbf{y}_j-\mathbf{y}_i|}\frac{\pi_i^\infty+\pi_j^\infty}{2}\left(\frac{\rho_j}{\pi_j^\infty}-\frac{\rho_i}{\pi_i^\infty}\right)\left(1+|\mathbf{y}_j-\mathbf{y}_i|\frac{(\boldsymbol{b}\cdot\boldsymbol{n})_{ij}^+\pi_i^\infty+(\boldsymbol{b}\cdot\boldsymbol{n})_{ji}^+\pi_j^\infty}{D(\pi_i^\infty+\pi_j^\infty)}\right) \tag{3.21}$$

has an additional numerical dissipation terms $\mathcal{O}\big(|\mathbf{y}_j-\mathbf{y}_i|\big)$. This numerical dissipation comes from the upwind discretization. Indeed, without this additional numerical dissipation term, $\partial_t\rho_i|C_i|=\sum_j L_{ij}$ is exactly the finite volume scheme designed in [18] for reversible case.

We remark that as long as we have Q-matrix structure, the ϕ-divergence dissipation holds. Indeed, let ϕ be a convex function and $E=\sum_i\phi\big(\frac{\rho_i}{\pi_i}\big)\pi_i$. Then using $\sum_j Q_{ji}\pi_j=0$ and $\sum_j Q_{ij}=0$ for any i, we have

$$\begin{aligned}\frac{\mathrm{d}}{\mathrm{d}t}\sum_i\rho_i\phi'\left(\frac{\rho_i}{\pi_i}\right)&=\sum_{i,j}Q_{ji}\rho_j\phi'\left(\frac{\rho_i}{\pi_i}\right)=\sum_{i,j,i\neq j}Q_{ji}\pi_j\frac{\rho_j}{\pi_j}\left(\phi'\left(\frac{\rho_i}{\pi_i}\right)-\phi'\left(\frac{\rho_j}{\pi_j}\right)\right)\\&=\sum_{i,j,j\neq i}Q_{ji}\pi_j\frac{\rho_j}{\pi_j}\left(\phi'\left(\frac{\rho_i}{\pi_i}\right)-\phi'\left(\frac{\rho_j}{\pi_j}\right)\right)-\sum_{i,j,j\neq i}Q_{ji}\pi_j\left(\psi\left(\frac{\rho_i}{\pi_i}\right)-\psi\left(\frac{\rho_j}{\pi_j}\right)\right)\\&=\sum_{i,j,j\neq i}Q_{ji}\pi_j\left(\frac{\rho_j}{\pi_j}\left(\phi'\left(\frac{\rho_i}{\pi_i}\right)-\phi'\left(\frac{\rho_j}{\pi_j}\right)\right)-\left(\psi\left(\frac{\rho_i}{\pi_i}\right)-\psi\left(\frac{\rho_j}{\pi_j}\right)\right)\right),\end{aligned} \tag{3.22}$$

where $\psi(x)$ is any function to be chosen later. Denote $y=\frac{\rho_j}{\pi_j}$ and $x=\frac{\rho_i}{\pi_i}$. To compute the Bregman divergence $D_\phi(y,x)$ associated with ϕ for points y,x, take $\psi(x)=x\phi'(x)-\phi(x)$, then $\psi'(x)=x\phi''(x)$ and

$$y[\phi'(x)-\phi'(y)]-[\psi(x)-\psi(y)]=(y-x)\phi'(x)+\phi(x)-\phi(y)=:-D_\phi(y,x). \tag{3.23}$$

Using the integral form of the reminder in Taylor expansion,

$$D_\phi(y,x)=(y-x)^2\int_0^1(1-\theta)\phi''(x+\theta(y-x))\,\mathrm{d}\theta\geq 0. \tag{3.24}$$

Then the dissipation relation becomes

$$\frac{\mathrm{d}E}{\mathrm{d}t}=-\sum_{i,j,j\neq i}Q_{ji}\pi_j D_\phi\left(\frac{\rho_j}{\pi_j},\frac{\rho_i}{\pi_i}\right)\leq 0. \tag{3.25}$$

3.2 Ergodicity

Let Q be the Q-matrix defined in (2.10). Recall the nonnegative irreducible stochastic matrix K defined in (3.2). Recall the right eigenvector $e:=(1,1,\cdots,1)^T$, i.e. $Ke=e$ corresponding to 1 and the left eigenvector, i.e. $\pi^T K=\pi^T$ due to the Perron-Frobenius theorem for K. We have the Jordan decomposition for K

$$K=S\begin{pmatrix}1&0\\0&J\end{pmatrix}S^{-1}=e\pi^T+S\begin{pmatrix}0&0\\0&J\end{pmatrix}S^{-1}, \tag{3.26}$$

where J consists of Jordan blocks with $|\mu_i|<1$, $i=2,\cdots,n$ and we used $S_{i1}=e_i$, $S^{-1}_{1j}=\pi_j$. Here and in the following context, the vector ρ^T is short for $\rho^T:=(\rho_1|C_1|,\cdots,\rho_n|C_n|)$.

Lemma 3.1. *Let Q be the Q-matrix defined in* (2.10) *and ρ_t be the solution to* (2.7)*. Given initial data ρ_0, we have*

$$\|\rho_t-\pi\|_{\ell^1}\le ce^{\frac{at}{2}(|\mu_2|-1)}\|\rho_0\|_{\ell^1}, \tag{3.27}$$

where $|\mu_2|<1$ is the second eigenvalue of Q and $a>0$ is the constant in (3.2).

Proof. From the construction for K and the Jordan decomposition in (3.26), we know

$$Q=a(K-I)=S\begin{pmatrix}0&0\\0&a(J-I)\end{pmatrix}S^{-1}. \tag{3.28}$$

Thus

$$e^{Qt}=e\pi^T+S\begin{pmatrix}0&0\\0&e^{a(J-I)t}\end{pmatrix}S^{-1}. \tag{3.29}$$

Then for the solution ρ_t to (2.7), we have

$$\rho_t^T-\pi^T=\rho_0^Te^{Qt}-\pi^T=\rho_0^TS\begin{pmatrix}0&0\\0&e^{a(J-I)t}\end{pmatrix}S^{-1}. \tag{3.30}$$

Notice J consists of Jordan blocks with $|\mu_i|<1$, $i=2,\cdots,n$, and each Jordan block ℓ can be written as the sum of $\mu_\ell I$ and a nilpotent matrix N. Thus we have $e^{at(J_\ell-I)}=e^{at(\mu_\ell-1)}e^{atN}$ and $\|e^{atN}\|_{\ell^1}\le ct^{n-2}$. Therefore, combining (3.30) with

$$\|e^{a(J-I)t}\|_{\ell^1}\le ct^{n-2}e^{at(|\mu_2|-1)}\le ce^{\frac{at(|\mu_2|-1)}{2}},$$

we conclude (3.27). □

Another proof for the ergodicity is using the following discrete mean Poincare's inequality [10, Lemma 10.2]. As a consequence, the exponential decay rate will not depend on the data size n.

Lemma 3.2 ([10]). *Assume $\sum_i u_i\pi_i|C_i|=0$, then we have the discrete mean Poincare inequality*

$$\sum_i u_i^2\pi_i|C_i|\le c\sum_{i,j}\frac{|\Gamma_{ij}|(\pi_i+\pi_j)}{|\mathbf{y}_i-\mathbf{y}_j|}\left(u_i-u_j\right)^2. \tag{3.31}$$

Using (3.15) in Proposition 3.1 and then taking $u_i=\frac{\rho_i}{\pi_i}-1$ in Lemma 3.2, we have

$$\frac{\mathrm{d}}{\mathrm{d}t}\sum_i\frac{(\rho_i-\pi_i)^2}{\pi_i}|C_i|\le-\frac{D}{2}\sum_{i,j}\frac{|\Gamma_{ij}|(\pi_i+\pi_j)}{|\mathbf{y}_i-\mathbf{y}_j|}\left(\frac{\rho_j}{\pi_j}-\frac{\rho_i}{\pi_i}\right)^2\le-c\sum_i\frac{(\rho_i-\pi)^2}{\pi_i}|C_i|. \tag{3.32}$$

This implies the exponential decay in χ^2-divergence

$$\sum_i\frac{(\rho_i-\pi_i)^2}{\pi_i}|C_i|\le e^{-ct}\sum_i\frac{(\rho_i(0)-\pi_i)^2}{\pi_i}|C_i|. \tag{3.33}$$

3.3 Unconditionally stable implicit scheme solved explicitly

Although there is no detailed balance property, we will use a mixed explicit-implicit time discretization to design an unconditionally stable mixed explicit-implicit scheme for (2.7), which enjoys a new stochastic-matrix structure. Since this scheme can be solved explicitly, we will also call it as an explicit scheme for simplicity.

Let $\rho_i^k|C_i|$ be the discrete density at the discrete time $k\Delta t$. Recall the constant $a>0$ and nonnegative irreducible matrix $K=\frac{Q}{a}+I$ defined in (3.2). Introduce the mixed explicit-implicit scheme as

$$\rho_i^{k+1}|C_i|-\rho_i^k|C_i|=\sum_j a\Delta t\left(K_{ji}\rho_j^k|C_j|-\rho_i^{k+1}|C_i|\right),\quad i=1,2,\cdots,n. \tag{3.34}$$

Now we recast it as a new discrete Markov chain with a transition probability $\tilde{K}$, which is unconditionally stable and enjoys fast convergence to the same steady state π. Rewrite (3.34) as

$$(1+a\Delta t)\rho_i^{k+1}|C_i|=a\Delta t\sum_j K_{ji}\rho_j^k|C_j|+\rho_i^k|C_i|=\Delta t\sum_j Q_{ji}\rho_j^k|C_j|+(1+a\Delta t)\rho_i^k|C_i|, \tag{3.35}$$

then we obtain a new Markov semigroup

$$\rho_i^{k+1}|C_i|=\frac{\Delta t}{1+a\Delta t}\sum_j Q_{ji}\rho_j^k|C_j|+\rho_i^k|C_i|=:\sum_j\tilde{K}_{ji}\rho_j^k|C_j|. \tag{3.36}$$

It is easy to verify

$$\tilde{K}=\Delta t\frac{Q}{1+a\Delta t}+I=:\Delta t\tilde{Q}+I \tag{3.37}$$

is a Markov semigroup operator and π being its positive invariant measure. Indeed, since

$$\tilde{K}=\frac{a\Delta t}{1+a\Delta t}\frac{Q}{a}+I,\quad \frac{a\Delta t}{1+a\Delta t}<1, \tag{3.38}$$

we know $\tilde{K}$ is always nonnegative, irreducible, aperiodic matrix and obtain the right eigenvector $e:=(1,1,\cdots,1)^T$, i.e. $\tilde{K}e=e$ corresponding to 1 and the left eigenvector, i.e. $\pi^T\tilde{K}=\pi^T$. From the Perron-Frobenius theorem, we have the Jordan decomposition for $\tilde{K}$

$$\tilde{K}=S\begin{pmatrix}1&0\\0&J\end{pmatrix}S^{-1}=e\pi^T+S\begin{pmatrix}0&0\\0&J\end{pmatrix}S^{-1}, \tag{3.39}$$

where J consists of Jordan blocks with $\tilde{K}$'s eigenvalues $|\mu_i|<1$, $i=2,\cdots,n$ and we used $S_{i1}=e_i$, $S^{-1}_{1j}=\pi_j$.

Therefore, thanks to $\tilde{Q}$-matrix, the explicit scheme (3.36) still enjoys good properties such as positive preserving, total mass preserving. Particularly, we give the following proposition for the unconditional ℓ^1-contraction and ergodicity.

Proposition 3.2 (Stability and ergodicity for fully discretized scheme)**.** Let Δt be the time step and let ρ^k be the solution to the explicit scheme (3.36). Then we have

(i) the ℓ^1 contraction, i.e., for any two solutions ρ^k,$\tilde{\rho}^k$,

$$\sum_i|\rho_i^{k+1}-\tilde{\rho}_i^{k+1}||C_i|\le\sum_i|\rho_i^n-\tilde{\rho}_i^n||C_i|; \tag{3.40}$$

(ii) the exponential convergence

$$\|\rho^k-\pi\|_{\ell^1}\le c\|\rho_0\|_{\ell^1}|\mu_2|^{k-n+2},\quad |\mu_2|<1, \tag{3.41}$$

where μ_2 is the second eigenvalue (in terms of the magnitude) of $\tilde{K}=I+\Delta t\frac{Q}{1+a\Delta t}$.

Proof. First, let ρ and $\tilde{\rho}$ be two solutions to (3.36). Denote $e_i^k=\rho_i^k-\tilde{\rho}_i^k$. Then (3.36) becomes

$$e_i^{k+1}|C_i|=\frac{\Delta t}{1+a\Delta t}\sum_j Q_{ij}e_j^k|C_j|+e_i^k|C_i|=\frac{\Delta t}{1+a\Delta t}\sum_{j\neq i}Q_{ij}e_j^k|C_j|+\left(1+\frac{Q_{ii}\Delta t}{1+a\Delta t}\right)e_i^k|C_i|. \tag{3.42}$$

From (3.38), each term above is nonnegative. Then take absolute value and summation in i to show that

$$\sum_i|e_i^{n+1}||C_i|\le\frac{\Delta t}{1+a\Delta t}\sum_{i,j}Q_{ij}|e_j^k||C_j|+\sum_i|e_i^k||C_i|=\sum_i|e_i^k||C_i|. \tag{3.43}$$

Second, (3.36) and the Jordan decomposition (3.39) yield

$$(\rho^k-\pi)^T=\rho_0^T\tilde{K}^k-\pi^T=\rho_0^TS\begin{pmatrix}0&0\\0&J^n\end{pmatrix}S^{-1}. \tag{3.44}$$

Then from $\|J^n\|_{\ell^1} \le c|\mu_2|^{k-n+2}$ and $\tilde{K}$'s second eigenvalue $|\mu_2|<1$, we conclude

$$\|\rho^k-\pi\|_{\ell^1} \le c\|\rho_0\|_{\ell^1}|\mu_2|^{k-n+2}. \tag{3.45}$$

This completes the proof. □

The advantage of this mixed implicit-explicit scheme (3.34) is that the Markov semigroup is always positive no matter how larger Δt is. However, when Δt becomes large, the spectral gap $1-|\mu_2|$ becomes small.

4 Convergence and error estimates

In this section, we present convergence and error estimates for the upwind scheme (2.6) including error estimates for numerical steady state solution π_i^∞ and the numerical dynamic solution $\rho_i(t)$. The estimates relies on the Taylor expansion along geodesic between each cell center and the discrete energy dissipation in Proposition 3.1. Same procedures can be done for π-symmetric upwind scheme and will be omitted.

4.1 Error estimate for steady state π

Let $\pi(\mathbf{y})$ be the exact solution to stationary Fokker-Planck equation (2.14) and let π_i be the numerical solution satisfying (3.7). In this section, for notation simplicity, we denote π_i as the numerical steady state π_i^∞. Plug the exact solution $\pi(\mathbf{y})$ into the numerical scheme and we estimate

$$\varepsilon_{ji}^{\pi} := \int_{\Gamma_{ij}} \mathbf{n}\cdot(D\nabla\pi-\boldsymbol{b}\pi)\,\mathrm{d}\mathcal{H}^{d-1} - F_{ji}^{\pi_{\mathrm{ex}}}, \tag{4.1}$$

where $\mathbf{n}$ is the restriction of the unit outward normal vector field on Γ_{ij}. Let $e_i := \pi_i-\pi(\mathbf{y}_i)$ be the error between the numerical steady state and the exact steady state. Then we have

$$\begin{aligned} &F_{ji}^e := F_{ji}^{\pi}-F_{ji}^{\pi_{\mathrm{ex}}} = |\Gamma_{ij}|\left(\frac{D(e_j-e_i)}{|\mathbf{y}_j-\mathbf{y}_i|}+(\boldsymbol{b}\cdot\boldsymbol{n})_{ij}^{-}e_j-(\boldsymbol{b}\cdot\boldsymbol{n})_{ij}^{+}e_i\right) = -F_{ij}^e, \\ &\sum_j F_{ji}^e = \sum_j \varepsilon_{ji}^{\pi}. \end{aligned} \tag{4.2}$$

Proposition 4.1. Let $e_i := \pi_i-\pi(\mathbf{y}_i)$ be the error between the numerical steady state π_i and the exact steady state $\pi(\mathbf{y}_i)$. Assume the Vonoroi tessellation satisfies

$$\sum_i \sum_{j\in VF(i)} |\Gamma_{ij}||\mathbf{y}_j-\mathbf{y}_i| \le c. \tag{4.3}$$

Then we have

$$\sum_i \frac{e_i^2}{\pi_i}|C_i| \le c\sum_{i,j}\frac{|\Gamma_{ij}|}{|\mathbf{y}_j-\mathbf{y}_i|}\left(\frac{e_j}{\pi_j}-\frac{e_i}{\pi_i}\right)^2 \le ch^2. \tag{4.4}$$

Proof. Step 1. Estimates for truncation error ε_{ji}^{π}.

Let G_{ij} be the bisector between $\mathbf{y}_i$ and $\mathbf{y}_j$, which is a $d-1$ submanifold containing Γ_{ij}. Suppose $\mathbf{y}^*$ is the intersection point of the geodesic from $\mathbf{y}_i$ to $\mathbf{y}_j$ and G_{ij}. We have $d_{\mathcal{N}}(\mathbf{y}^*,\mathbf{y}_i)=d_{\mathcal{N}}(\mathbf{y}^*,\mathbf{y}_j)$. Notice the unit tangent vector of the geodesic at $\mathbf{y}^*$ is perpendicular to Γ_{ij} at $\mathbf{y}^*$ and can be chosen as the unit normal $\boldsymbol{n}_{ij}(\mathbf{y}^*)$[§]. From the Taylor expansion of π along the geodesic, we have

$$\pi(\mathbf{y}_j)-\pi(\mathbf{y}^*)=\boldsymbol{n}_{ij}\cdot\nabla\pi(\mathbf{y}^*)d_{\mathcal{N}}(\mathbf{y}^*,\mathbf{y}_j)+\mathcal{O}(d_{\mathcal{N}}^2(\mathbf{y}^*,\mathbf{y}_j)), \tag{4.5}$$

$$\pi(\mathbf{y}^*)-\pi(\mathbf{y}_i)=\boldsymbol{n}_{ij}\cdot\nabla\pi(\mathbf{y}^*)d_{\mathcal{N}}(\mathbf{y}^*,\mathbf{y}_i)+\mathcal{O}(d_{\mathcal{N}}^2(\mathbf{y}^*,\mathbf{y}_i)). \tag{4.6}$$

Therefore, if we add the above two equations, we have

$$\pi(\mathbf{y}_j)-\pi(\mathbf{y}_i)=\mathbf{n}_{ij}\cdot\nabla\pi(\mathbf{y}^*)d_{\mathcal{N}}(\mathbf{y}_i,\mathbf{y}_j)+\mathcal{O}(d_{\mathcal{N}}^2(\mathbf{y}_i,\mathbf{y}_j)). \tag{4.7}$$

Hence,

$$\mathbf{n}_{ij}\cdot\nabla\pi(\mathbf{y}^*)=\frac{\pi(\mathbf{y}_j)-\pi(\mathbf{y}_i)}{d_{\mathcal{N}}(\mathbf{y}_i,\mathbf{y}_j)}+\mathcal{O}(d_{\mathcal{N}}(\mathbf{y}_i,\mathbf{y}_j))=\frac{\pi(\mathbf{y}_j)-\pi(\mathbf{y}_i)}{|\mathbf{y}_i-\mathbf{y}_j|}+\mathcal{O}(d_{\mathcal{N}}(\mathbf{y}_i,\mathbf{y}_j)), \tag{4.8}$$

where we used $|\mathbf{y}_i-\mathbf{y}_j|=d_{\mathcal{N}}(\mathbf{y}_i,\mathbf{y}_j)+o(d_{\mathcal{N}}(\mathbf{y}_i,\mathbf{y}_j))$ for $d_{\mathcal{N}}(\mathbf{y}_i,\mathbf{y}_j)$ small enough. Similarly,

$$\pi(\mathbf{y}_j)-\pi(\mathbf{y}^*)=\mathcal{O}(d_{\mathcal{N}}(\mathbf{y}^*,\mathbf{y}_j)), \tag{4.9}$$

$$\pi(\mathbf{y}^*)-\pi(\mathbf{y}_i)=\mathcal{O}(d_{\mathcal{N}}(\mathbf{y}^*,\mathbf{y}_i)). \tag{4.10}$$

Hence we have

$$\left(-(\boldsymbol{b}\cdot\boldsymbol{n})_{ij}^{+}+(\boldsymbol{b}\cdot\boldsymbol{n})_{ij}^{-}\right)\pi(\mathbf{y}^*)=-(\boldsymbol{b}\cdot\boldsymbol{n})_{ij}^{+}\pi(\mathbf{y}_i)+(\boldsymbol{b}\cdot\boldsymbol{n})_{ij}^{-}\pi(\mathbf{y}_j)+\mathcal{O}(d_{\mathcal{N}}(\mathbf{y}_i,\mathbf{y}_j)). \tag{4.11}$$

Thus if $\mathbf{y}^*$ is changes to any $\mathbf{y}$ on Γ_{ij},

$$\mathcal{O}(d_{\mathcal{N}}(\mathbf{y}_i,\mathbf{y})+d_{\mathcal{N}}(\mathbf{y}_i,\mathbf{y}_j))=\mathcal{O}(\mathrm{diam}(C_i)+d_{\mathcal{N}}(\mathbf{y}_i,\mathbf{y}_j))\leq\mathcal{O}(h),$$

where

$$h:=\max\Big(\max_{i=1,\cdots,n}(\mathrm{diam}(C_i)),\max_{i=1,\ldots,n}\big(\max_{j\in VF(i)}d_{\mathcal{N}}(\mathbf{y}_i,\mathbf{y}_j)\big)\Big). \tag{4.12}$$

This, together with (4.8) and (4.11), we conclude

$$\varepsilon_{ij}^{\pi}\leq ch|\Gamma_{ij}|. \tag{4.13}$$

Step 2. H^1 estimates via anti-symmetric structure.

[§]on the $d-1$ dimensional submanifold containing Γ_{ij}

Using same derivations as Proposition 3.1, we have

$$\sum_i \left(\frac{e_i}{\pi_i} \sum_j F^e_{ji} \right) = -\frac{1}{2} \sum_{i,j} \alpha_{ij} \left(\frac{e_j}{\pi_j} - \frac{e_i}{\pi_i} \right)^2, \tag{4.14}$$

where α_{ij} defined in (3.16). And thus (4.2) implies

$$\sum_i \left(\frac{e_i}{\pi_i} \sum_j F^e_{ji} \right) = \sum_{i,j} \varepsilon^\pi_{ji} \frac{e_i}{\pi_i} = \frac{1}{2} \sum_{i,j} \varepsilon^\pi_{ji} \left(\frac{e_i}{\pi_i} - \frac{e_j}{\pi_j} \right). \tag{4.15}$$

Then combining this with (4.14) and Young's inequality, we know

$$\sum_{i,j} \alpha_{ij} \left(\frac{e_j}{\pi_j} - \frac{e_i}{\pi_i} \right)^2 = -\sum_{i,j} \varepsilon^\pi_{ji} \left(\frac{e_i}{\pi_i} - \frac{e_j}{\pi_j} \right) \le \frac{1}{2} \sum_{i,j} \alpha_{ij} \left(\frac{e_i}{\pi_i} - \frac{e_j}{\pi_j} \right)^2 + \frac{1}{2} \sum_{i,j} \frac{(\varepsilon^\pi_{ji})^2}{\alpha_{ij}}. \tag{4.16}$$

Then by (4.13) and (3.19), we conclude

$$\sum_{i,j} \alpha_{ij} \left(\frac{e_j}{\pi_j} - \frac{e_i}{\pi_i} \right)^2 \le \sum_{i,j} \frac{(\varepsilon^\pi_{ji})^2}{\alpha_{ij}} \le ch^2 \sum_{i,j} |\Gamma_{ij}| |\mathbf{y}_j - \mathbf{y}_i| \le ch^2. \tag{4.17}$$

Moreover, since $\sum_i e_i |C_i| = 0$, we take $u_i = \frac{e_i}{\pi_i}$ in Lemma 3.2 to obtain

$$\sum_i \frac{e_i^2}{\pi_i} |C_i| \le c \sum_{i,j} \alpha_{ij} \left(\frac{e_j}{\pi_j} - \frac{e_i}{\pi_i} \right)^2 \le ch^2. \tag{4.18}$$

This, together with the definition of α_{ij} in (3.16), concludes (4.4). □

4.2 Convergence of dynamic solution in χ^2-discrepancy

Let $\rho_t(\mathbf{y})$ be the exact solution to (1.2). Let $e_i(t) := \rho_t(\mathbf{y}_i) - \rho_i(t)$ be the error between the exact solution and the numerical solution. Now for any fixed $T > 0$, we give the convergence result in terms of the χ^2-discrepancy between the exact solution and the numerical solution.

Theorem 4.1. *Let $e_i(t) := \rho_i(t) - \rho_t(\mathbf{y}_i)$ be the error between the numerical solution $\rho_i(t)$ and the exact steady state $\rho_t(\mathbf{y}_i)$. Assume the Vonoroi tessellation satisfies* (4.3)*, then for any $T > 0$ and h defined in* (4.12)*, we have*

$$\max_{t \in [0,T]} \sum_i \frac{e_i(t)^2}{\pi_i} |C_i| \le \left(\sum_i \frac{e_i(0)^2}{\pi_i} |C_i| + \mathcal{O}(h^2) \right) e^T. \tag{4.19}$$

Proof. Let $\rho_i^e := \frac{1}{|C_i|}\int_{C_i}\rho\,\mathrm{d}y$ be the cell average. Plug the exact solution into the numerical scheme

$$\begin{aligned}\partial_t(\rho_i^e|C_i|) &= \sum_{j\in VF(i)} F_{ji}^{ex} + \sum_{j\in VF(i)}\varepsilon_{ji},\\ \varepsilon_{ji} &:= \int_{\Gamma_{ij}} \mathbf{n}\cdot(D\nabla\rho - \boldsymbol{b}\rho)\,\mathrm{d}\mathcal{H}^{d-1} - F_{ji}^{ex},\end{aligned} \tag{4.20}$$

where $\mathbf{n}$ is the restriction of the unit outward normal vector field on Γ_{ij} and

$$F_{ji}^{ex} := \frac{1}{2}\alpha_{ij}\left(\frac{\rho(\mathbf{y}_j)}{\pi_j} - \frac{\rho(\mathbf{y}_i)}{\pi_i}\right) + \frac{F_{ji}^{\pi}}{2}\left(\frac{\rho(\mathbf{y}_i)}{\pi_i} + \frac{\rho(\mathbf{y}_j)}{\pi_j}\right) \tag{4.21}$$

with α_{ij} defined in (3.16). Exchanging i,j above, we see both ε_{ji} and F_{ji}^{ex} are anti-symmetric.

Subtracting the numerical scheme (2.6) from (4.20), we have

$$\frac{\mathrm{d}}{\mathrm{d}t}e_i|C_i| = \sum_{j\in VF(i)}\left(\frac{\alpha_{ij}}{2}\left(\frac{e_j}{\pi_j} - \frac{e_i}{\pi_i}\right) + \frac{F_{ji}^{\pi}}{2}\left(\frac{e_i}{\pi_i} + \frac{e_j}{\pi_j}\right)\right) + \sum_{j\in VF(i)}\varepsilon_{ji} + \partial_t(\rho(\mathbf{y}_i) - \rho_i^e)|C_i|. \tag{4.22}$$

Similar to the derivation of dissipation relation (3.14), we multiply this by $\frac{2e_i}{\pi_i}$ and use (3.7) to show that

$$\frac{\mathrm{d}}{\mathrm{d}t}\sum_i \frac{e_i^2}{\pi_i}|C_i| = -\sum_{i,j}\frac{\alpha_{ij}}{2}\left(\frac{e_j}{\pi_j} - \frac{e_i}{\pi_i}\right)^2 + \sum_{i,j}\varepsilon_{ji}\left(\frac{e_i}{\pi_i} - \frac{e_j}{\pi_j}\right) + \sum_i 2\partial_t(\rho(\mathbf{y}_i) - \rho_i^e)|C_i|\frac{e_i}{\pi_i}, \tag{4.23}$$

due to $\varepsilon_{ij} = -\varepsilon_{ji}$. Applying Young's inequality to the last two terms, we have

$$\begin{aligned}&\sum_{i,j}\varepsilon_{ji}\left(\frac{e_i}{\pi_i} - \frac{e_j}{\pi_j}\right) \le \sum_{i,j}\frac{\alpha_{ij}}{4}\left(\frac{e_j}{\pi_j} - \frac{e_i}{\pi_i}\right)^2 + \sum_i\sum_{j\in VF(i)}\frac{\varepsilon_{ji}^2}{\alpha_{ij}};\\ &\sum_i 2\partial_t(\rho(\mathbf{y}_i) - \rho_i^e)|C_i|\frac{e_i}{\pi_i} \le \sum_i[\partial_t(\rho(\mathbf{y}_i) - \rho_i^e)]^2\frac{|C_i|}{\pi_i} + \sum_i\frac{e_i^2}{\pi_i}|C_i|.\end{aligned} \tag{4.24}$$

Thus we have

$$\frac{\mathrm{d}}{\mathrm{d}t}\sum_i\frac{e_i(t)^2}{\pi_i}|C_i| \le \sum_{i,j}\frac{\varepsilon_{ji}^2}{\alpha_{ij}} + \sum_i[\partial_t(\rho(\mathbf{y}_i) - \rho_i^e)]^2\frac{|C_i|}{\pi_i} + \sum_i\frac{e_i^2}{\pi_i}|C_i|. \tag{4.25}$$

The estimates for ε_{ji} and $\partial_t(\rho(\mathbf{y}_i) - \rho_i^e)$ using Taylor expansion on manifold are same as (4.13). From (4.13) and (3.19), we have

$$\frac{\varepsilon_{ji}^2}{\alpha_{ij}} \le ch^2|\mathbf{y}_j - \mathbf{y}_i||\Gamma_{ij}|. \tag{4.26}$$

From the assumption (4.3), we know

$$\sum_{i,j}\frac{\varepsilon_{ji}^2}{\alpha_{ij}}\leq ch^2. \tag{4.27}$$

By Gronwall's inequality, we obtain for any $T>0$,

$$\max_{t\in[0,T]}\sum_i\frac{e_i(t)^2}{\pi_i}|C_i|\leq\left(\sum_i\frac{e_i(0)^2}{\pi_i}|C_i|+\mathcal{O}(h^2)\right)e^T. \tag{4.28}$$

This completes the proof. □

We remark that for numerical solution itself, the exponential convergence to the numerical invariant measure (which recovers exact invariant measure) is proved in Section 3. However, the error between the exact solution and the numerical solution still depends on e^T as long as one use Gronwall's inequality in the error estimate. With the well-balanced property in (2.40), it is possible to obtain a uniform error estimate but we leave it for the future study.

5 Numerical examples

In this section, we demonstrate three examples based on two upwind schemes developed in Section 2. Section 5.1 focus on the case that we know information of an invariant measure π. In realistic situations, knowing the output of π from a computer code instead of an analytic formula is enough. In this case, we use π-symmetric upwind scheme (2.27) to conduct two interesting applications: (i) efficient sampling enhanced by an incompressible mixture flow (ii) image transformations immersed in a mixture flow. Section 5.2 focus on the case we only know the drift vector field $\boldsymbol{b}$ in the irreversible drift-diffusion process (1.4) and we adapt the numerical scheme (2.6) to solve both a steady state solution and simulate the irreversible dynamics. The π-symmetric upwind scheme (A.8) and upwind scheme (A.15) for a 2D structured grids case with no-flux boundary conditions are given in Appendix A.1 and Appendix A.2 for completeness.

5.1 Simulations for irreversible dynamics given an invariant measure

In this section, assume we know the output of an invariant measure π, which could be a steady state in a biochemical process, or a given target density function in sampling, or given images. We will use π-symmetric upwind scheme (2.27) for a 2D structured grids to demonstrate two examples.

5.1.1 Example: Sampling enhanced by an incompressible mixture flow

Take 2D domain as $\Omega=[a,b]\times[c,d]=[-4.5,4.5]\times[-4.5,4.5]$. Choose the stream function for a 2D sinusoidal cellular flow

$$\psi(x,y):=A\sin\frac{k\pi(x-a)}{b-a}\sin\frac{k\pi(y-c)}{d-c}, \tag{5.1}$$

where A represents the amplitude of the mixture velocity $\boldsymbol{u}$ and k is the normalized wave number of the mixture. Then the incompressible velocity field

$$\boldsymbol{u}=\begin{pmatrix}-\partial_y\psi\\ \partial_x\psi\end{pmatrix}$$

can be discretized using (2.37).

Now we use (2.39), i.e., (A.8) for 2D structured grids, to sample a given target density: a smiling triple-banana in (5.2). Based on the Laplace principle, we can use the smooth minimum method to construct a smiling triple-banana as a target density

$$\begin{aligned}\pi(x,y)\propto\ & e^{-20\left[\left(x-\frac{6}{5}\right)^2+\left(y-\frac{6}{5}\right)^2-\frac{1}{2}\right]^2+\log\left(e^{-10(y-2)^2}\right)}+e^{-20\left[\left(x+\frac{6}{5}\right)^2+\left(y-\frac{6}{5}\right)^2-\frac{1}{2}\right]^2+\log\left(e^{-10(y-2)^2}\right)}\\ &+e^{-20\left(x^2+y^2-2\right)^2+\log\left(e^{-10(y+1)^2}\right)}+0.1;\end{aligned} \tag{5.2}$$

see Fig. 1(right). Then we take a Gaussian mixture

$$\rho_0(x,y)\propto e^{-16(x+3)^2-4y^2}+e^{-16(x-3)^2-4y^2}+e^{-4x^2-16(y+3)^2}+e^{-4x^2-16(y-3)^2}+0.1 \tag{5.3}$$

as an initial density; see Fig. 1(left). Set the computational parameters as diffusion constant $D=0.5$, time step $\Delta t=0.01$, uniform grid size $\Delta x=\Delta y=0.09$. Then with the amplitude of the mixture velocity A=0.1 and the frequency k=8, the time evolution of dynamic

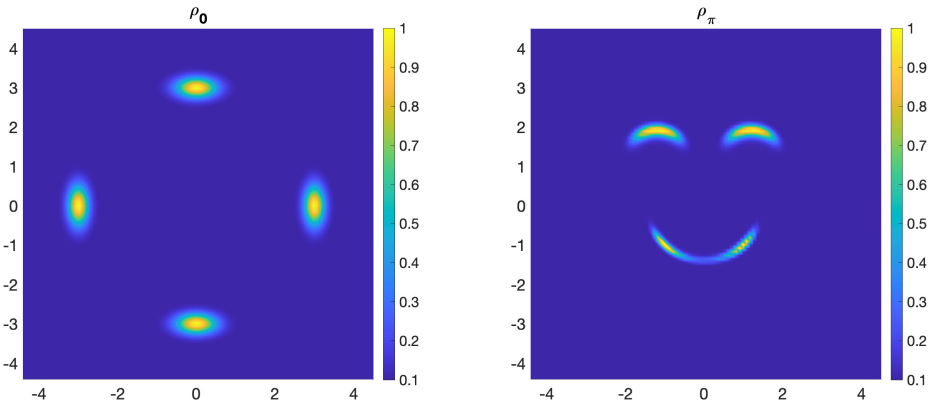

Figure 1: The normalized initial density (left) and the target density: smiling triple banana (right).

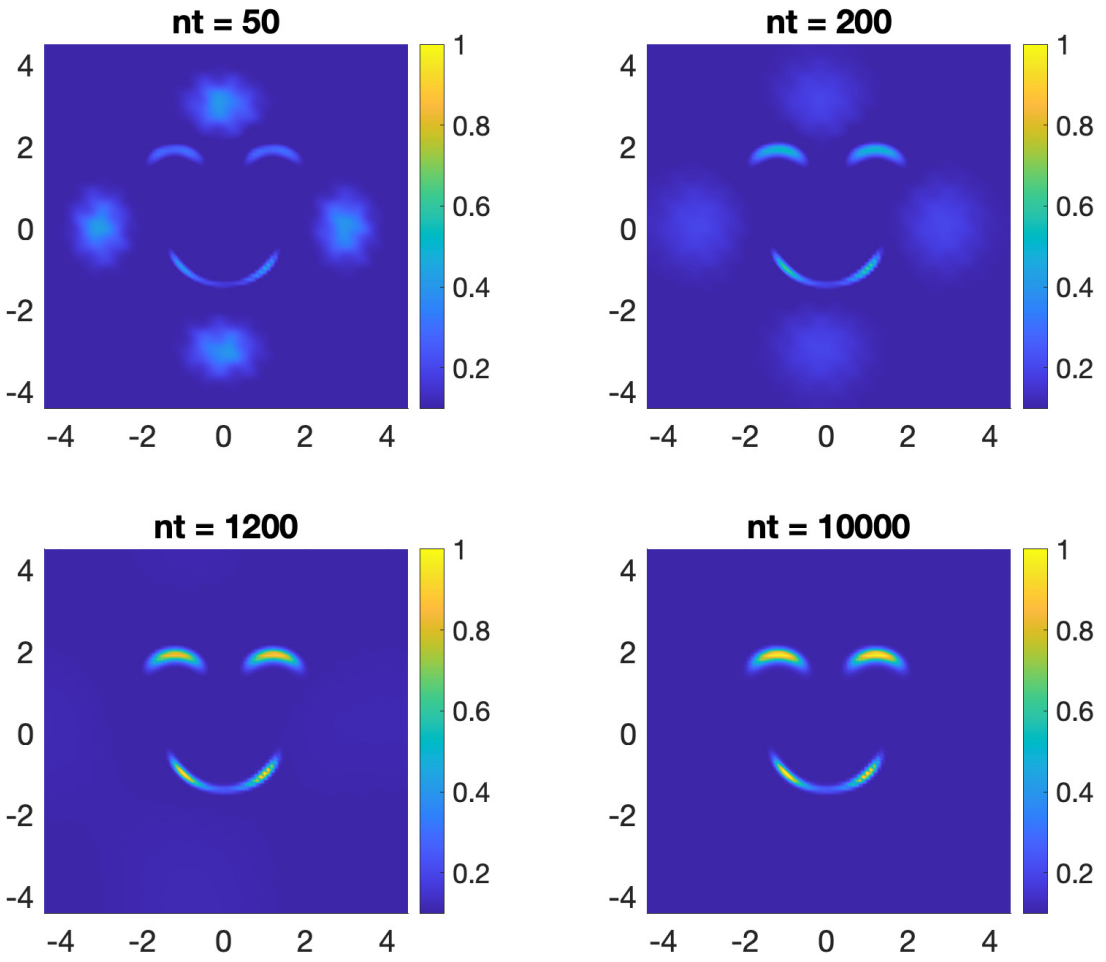

Figure 2: The time evolution of dynamic solution for sampling the smiling triple banana using (2.39). The amplitude of the mixture velocity is $A=0.1$ and snapshots are shown at iterations $n_t=50,200,1200,10000$.

density ρ_t is shown at time iteration $n_t=50,200,1200,10000$ in Fig. 2. Moreover, the relative root mean square error between the dynamic solution ρ_t and the target density π are shown w.r.t time iterations using semilog plot in Fig. 3 with different amplitude of the mixture velocity $A=0$ and 0.1. Notice if $A=0$, then the Fokker-Planck equation (2.15) and the corresponding upwind scheme (2.39) are reduced to the reversible case, i.e., we only have the gradient flow part in (2.15). The corresponding Q-matrix for the reversible case ($\boldsymbol{u}=0$) of course also leads to an efficient sampling for the target density. However, the additional incompressible convection with larger mixture velocity $\boldsymbol{u}$, although makes the dynamics irreversible, can speed up the convergence to the target density function. This observation is shown in the semilog plot in Fig. 3 for the decay of the relative root mean square error with amplitude $A=0.1$, compared with $A=0$. The enhanced convergence and diffusion by a mixture velocity filed is a classical topic in the fluid dynamics and

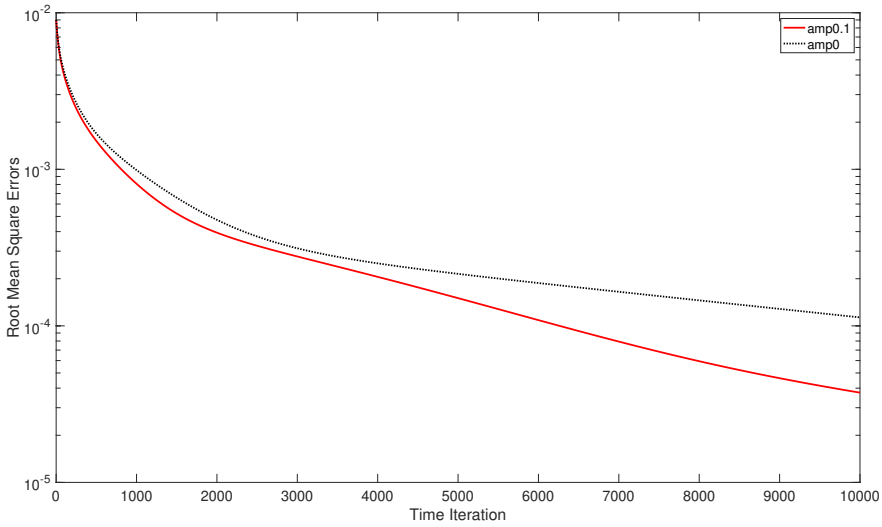

Figure 3: The relative root mean square error between the dynamic density and the target triple banana density is shown in semilog plot w.r.t time iterations. With different amplitude $A=0$ and 0.1, we observe the enhancement of convergence brought by the incompressible mixture velocity $\boldsymbol{u}$.

PDE analysis [8, 11]. This technique has a promising applications in sampling, Markov chain Monte Carlo and non-convex optimizations. We will leave this line of research as a future study.

5.1.2 Example: image transformation immersed in an incompressible flow

In this example, we use van Gogh's 'The Starry Night' to simulate an image immersed in an irreversible dynamics but still converge to a given target image. Choose an initial image with the same village view but with a purely blue sky, as shown in Fig. 4(left). The target image 'The Starry Night' is shown in Fig. 4(right). Each matrix exacted from these two images contains values of a color mode (R or G or B) and are both $N=256$ pixels in width and $M=203$ pixels in height.

Set the computational parameters as diffusion constant $D=0.4$, time step $\Delta t=0.01$, uniform grid size $\Delta x=\frac{\pi}{N}, \Delta y=\frac{\pi}{M}$. Then with the amplitude of the mixture velocity $A=1000$ and the normalized wave number $k=8$, the time evolution of dynamic density ρ_t is shown at time iteration $n_t=5,80,400,2000$ in Fig. 5. Starting from a purely blue sky, we can see the night sky immersed in the incompressible flow, which is discretized using (2.37) with (5.1), becomes starry, unbalanced and distorted. At $n_t=2000$, the image is very close to the target image while the more unbalanced inbetweening image is shown at $n_t=400$. Moreover, the relative root mean square error between the dynamic solution ρ_t and the target density π are shown w.r.t time iterations using semilog plot in Fig. 6. We still observe that larger amplitude of the mixture velocity has an enhancement for the convergence of dynamic solution to its steady state.

Figure 4: The initial image (left) and the target image: The Starry Night (right).

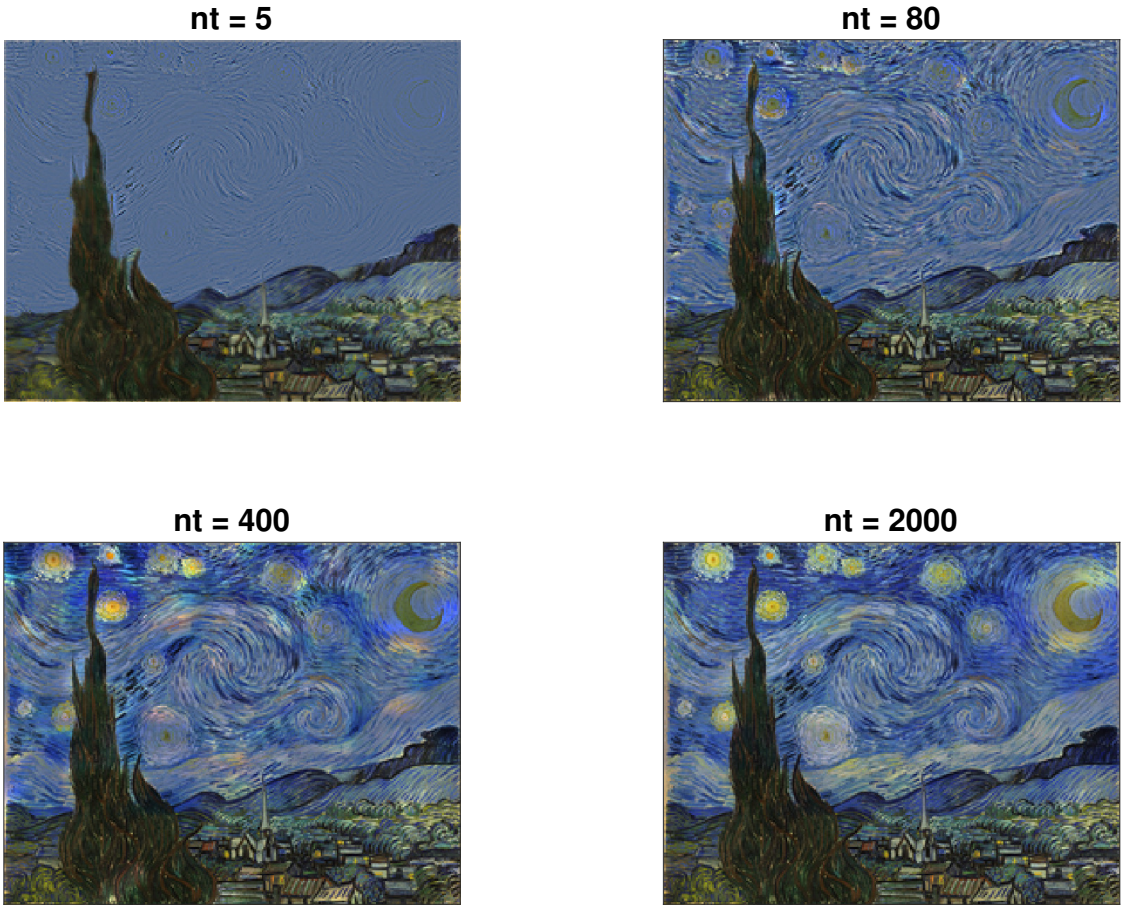

Figure 5: The time evolution of image transformations immersed in an incompressible flow using scheme (2.39). The amplitude of the mixture velocity is $A=1000$ and snapshots are shown at iterations $n_t=5,80,400,2000$.

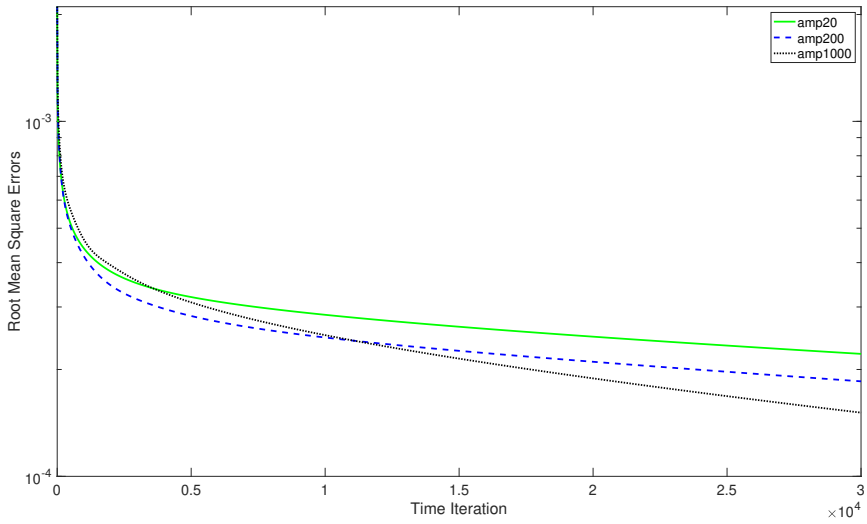

Figure 6: The relative root mean square error between the dynamic image in blue color-modes and the target image is shown in semilog plot w.r.t time iterations. Enhanced convergence is shown with different amplitude $A=20,200,1000$.

5.2 Simulations for general irreversible dynamics without information of invariant measure

In this section, assume in irreversible drift-diffusion process (1.4), we only know the drift vector field $\boldsymbol{b}$. Then we use the upwind scheme (2.6) in 2D structured grids to simulate a stochastic Van der Pol oscillator.

5.2.1 Example: Stochastic Van der Pol oscillator model

The famous Van der Pol model is first proposed by Van der Pol to describe electrical circuit and also has numerous extended applications in biology, pharmacology and seismology. For instance the FitzHugh-Nagumo model describing the excitation and propagation of sodium and potassium ions in a neuron [22]. There are lots of classical investigations on the limit circle, bifurcations and chaos on this model; c.f. [34].

To illustrate our numerical scheme for the irreversible dynamics without steady state information, consider a stochastic version of Van der Pol oscillator model

$$\begin{aligned} \mathrm{d}x &= \alpha\left(x-\frac{x^3}{3}+y\right)\mathrm{d}t+\sqrt{2\varepsilon}\mathrm{d}B; \\ \mathrm{d}y &= (\delta-x)\,\mathrm{d}t+\sqrt{2\varepsilon}\mathrm{d}B \end{aligned} \tag{5.4}$$

with a set of classical parameters $\alpha=10$ and $\delta=0$ or $\delta=1$. After adding the Brownian motion with $\varepsilon>0$, this is a typical example which can be decomposed as a gradient flow part and a Hamiltonian part.

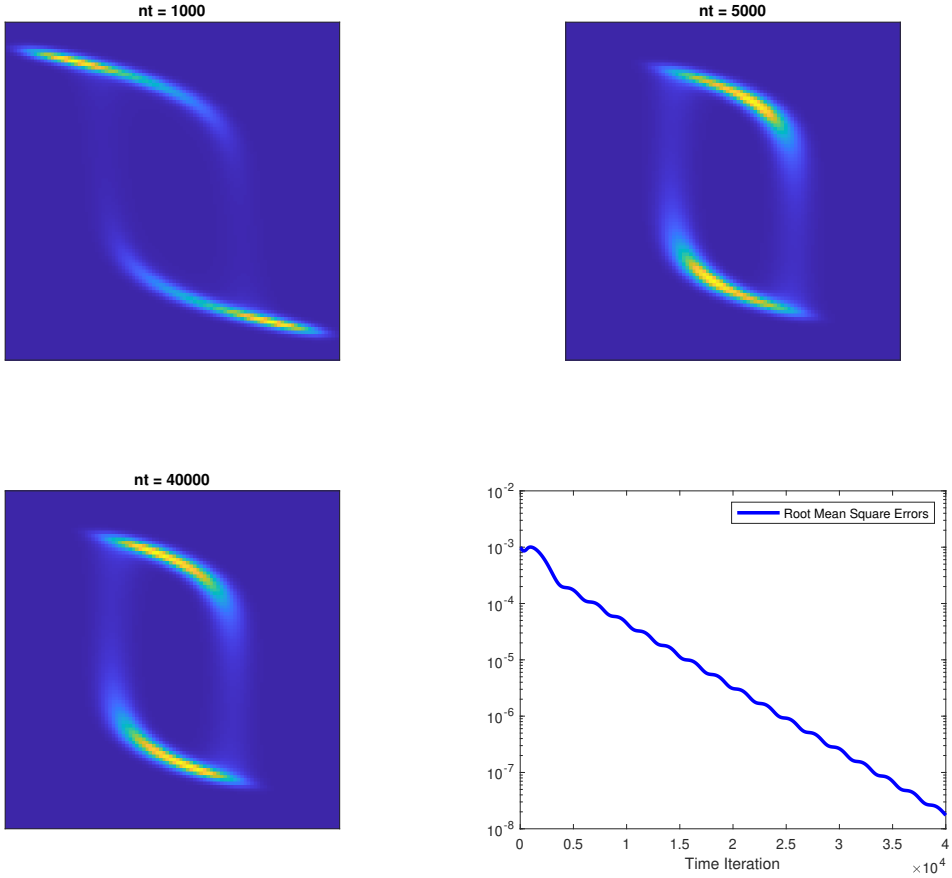

Figure 7: The time evolution of density function to (5.5) with $\delta=0$. At time iteration $n_t=40000$, the steady state tends to concentrate near the larger limit circle (bottom left). The root mean square error between the numerical solution ρ_t and the numerical steady state π^∞ is shown in the semilog plot (bottom right).

The corresponding Fokker-Planck equation is

$$\partial_t\rho=\nabla\cdot(\varepsilon\nabla\rho-\boldsymbol{b}\rho);\quad \boldsymbol{b}=\left(\alpha\left(x-\frac{x^3}{3}+y\right),(\delta-x)\right). \tag{5.5}$$

We take domain as $\Omega=[-3,4]\times[-3,3]$, noise level as $\varepsilon=0.1$, computational parameters as $\Delta t=0.05$, $\Delta x=0.07,\Delta y=0.06$ and take the no-flux boundary condition (A.13). Then based on (3.35) (i.e., (A.15)), starting from the initial density $\rho_0=0.2$, we compute the time evolution of the density function ρ_t.

With parameter $\delta=0$, the numerical solution at time iteration $n_t=1000,5000,40000$ are shown in Fig. 7. Meanwhile, the numerical steady state π^∞ is computed by setting the time iteration as $n_t=200000$, because in Proposition 4.1 we have proved the exponential ergodicity for the unconditionally explicit scheme (3.36). The root mean square error between the numerical solution ρ_t and the numerical steady state π^∞ is shown in the

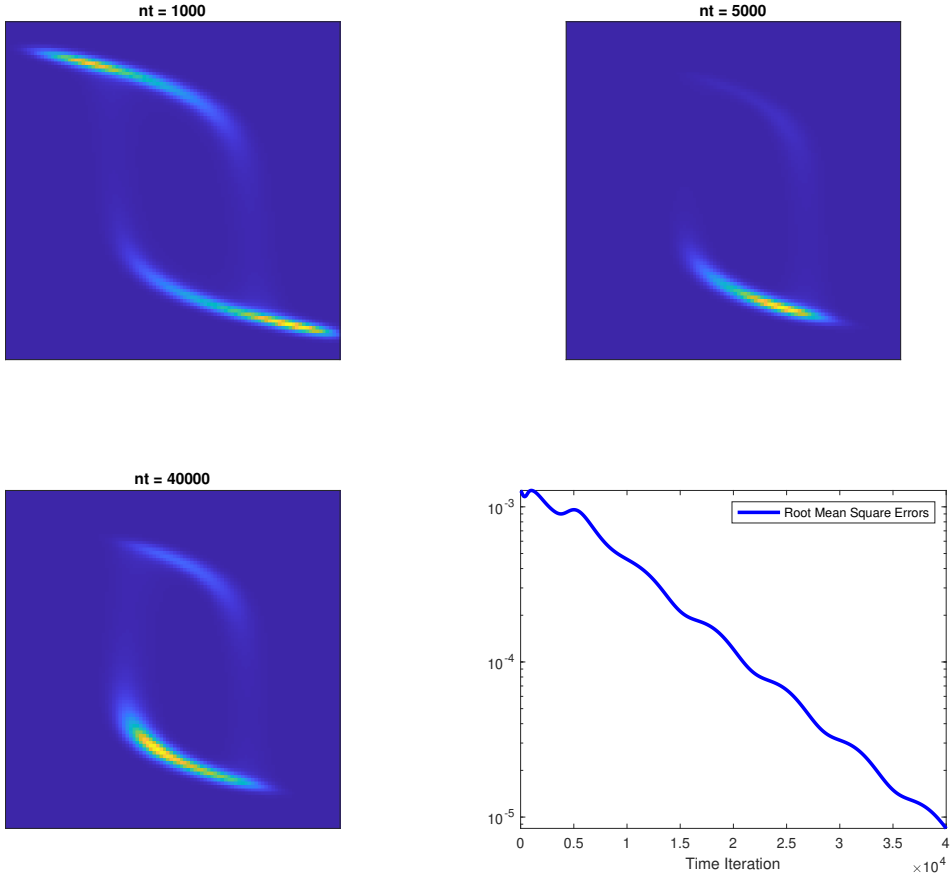

Figure 8: The time evolution of density function to (5.5) with $\delta = 1$. The steady state tends to concentrate near the smaller limit circle (bottom left). In terms of time iterations, the root mean square error between the numerical solution ρ and the numerical steady state π is shown in the semilog plot (bottom right).

semilog plot in Fig. 7(bottom right) in terms of time iterations. We can see for $\delta = 0$, the steady state density tends to concentrate near a large limit circle in Fig. 7(bottom left), which is the stable limit circle for the deterministic Van der Pol oscillator in the large damping regime (a.k.a. relaxation oscillation).

As a comparison, with different parameter $\delta = 1$, the numerical solution at time iteration $n_t = 1000,5000,40000$ are shown in Fig. 8. The root mean square error between the numerical solution ρ and the numerical steady state π^∞ is shown in the semilog plot in Fig. 8(bottom right), where the numerical steady state is still obtained by setting the time iteration as $n_t = 200000$. We can see clearly the steady state density now concentrates near a smaller region in Fig. 8(bottom left). Indeed, this small region is near another smaller limit circle for the deterministic Van der Pol oscillator, but due to the random noise, the steady state density does not exactly concentrate only on the smaller limit circle.

Acknowledgments

Jian-Guo Liu was supported in part by NSF under awards DMS-2106988 and by NSF RTG grant DMS-2038056. Yuan Gao was supported by NSF under awards DMS-2204288.

A Finite volume scheme for 2D structured grids

A.1 π-symmetric upwind scheme in 2D with a given invariant measure

After choosing $\boldsymbol{u}$ satisfying (2.37), we use (2.39) to present the π-symmetric upwind scheme in a structured 2D domain $\Omega:=[a,b]\times[c,d]$.

(i) Define the rectangle cells as

$$C_{ij}=((i-1)\Delta x,i\Delta x)\times((j-1)\Delta y,j\Delta y),\quad i=1,\cdots,N,\ j=1,\cdots,M. \tag{A.1}$$

Denote the approximated density on C_{ij} as $\rho_{i,j}$; Denote the cell centers (x_i,y_j) as

$$x_i=a+\Big(i-\frac{1}{2}\Big)\Delta x,\quad y_j=c+\Big(j-\frac{1}{2}\Big)\Delta y,\quad i=1,\cdots,N,\ j=1,\cdots,M. \tag{A.2}$$

(ii) Denote the discrete drift $(\boldsymbol{u}\cdot\boldsymbol{n})_{i,j}|\Gamma_{i,j}|$ of cell C_{ij} on each (right/left/up/down) faces Γ_{ij} along outer normal $\boldsymbol{n}$ as

$$\begin{aligned}
(\boldsymbol{u}\cdot\boldsymbol{n})^R_{i,j}\Delta y&=\psi\Big(x_i+\frac{\Delta x}{2},y_j+\frac{\Delta y}{2}\Big)-\psi\Big(x_i+\frac{\Delta x}{2},y_j-\frac{\Delta y}{2}\Big),\\
(\boldsymbol{u}\cdot\boldsymbol{n})^L_{i,j}\Delta y&=\psi\Big(x_i-\frac{\Delta x}{2},y_j-\frac{\Delta y}{2}\Big)-\psi\Big(x_i-\frac{\Delta x}{2},y_j+\frac{\Delta y}{2}\Big),\\
(\boldsymbol{u}\cdot\boldsymbol{n})^U_{i,j}\Delta x&=\psi\Big(x_i-\frac{\Delta x}{2},y_j+\frac{\Delta y}{2}\Big)-\psi\Big(x_i+\frac{\Delta x}{2},y_j+\frac{\Delta y}{2}\Big),\\
(\boldsymbol{u}\cdot\boldsymbol{n})^D_{i,j}\Delta x&=\psi\Big(x_i+\frac{\Delta x}{2},y_j-\frac{\Delta y}{2}\Big)-\psi\Big(x_i-\frac{\Delta x}{2},y_j-\frac{\Delta y}{2}\Big).
\end{aligned}$$

(iii) Based on (2.39), using the negative part of the discrete drift above, define the inward flux F into cell C_{ij} from four cell faces (right/left/up/down) Γ_{ij} as

$$\begin{aligned}
F^{\mathrm{R}}_{i,j}&=\Delta y\left(\frac{D(\pi_{i+1,j}+\pi_{i,j})}{2\Delta x}+(\boldsymbol{u}\cdot\boldsymbol{n})^{R-}_{i,j}\right)\left(\frac{\rho_{i+1,j}}{\pi_{i+1,j}}-\frac{\rho_{i,j}}{\pi_{i,j}}\right),\\
F^{\mathrm{L}}_{i,j}&=\Delta y\left(\frac{D(\pi_{i-1,j}+\pi_{i,j})}{2\Delta x}+(\boldsymbol{u}\cdot\boldsymbol{n})^{L-}_{i,j}\right)\left(\frac{\rho_{i-1,j}}{\pi_{i-1,j}}-\frac{\rho_{i,j}}{\pi_{i,j}}\right),\ \ i=2,\cdots,N-1,\ j=1,\cdots,M;\\
F^{\mathrm{U}}_{i,j}&=\Delta x\left(\frac{D(\pi_{i,j+1}+\pi_{i,j})}{2\Delta y}+(\boldsymbol{u}\cdot\boldsymbol{n})^{U-}_{i,j}\right)\left(\frac{\rho_{i,j+1}}{\pi_{i,j+1}}-\frac{\rho_{i,j}}{\pi_{i,j}}\right),\\
F^{\mathrm{D}}_{i,j}&=\Delta x\left(\frac{D(\pi_{i,j-1}+\pi_{i,j})}{2\Delta y}+(\boldsymbol{u}\cdot\boldsymbol{n})^{D-}_{i,j}\right)\left(\frac{\rho_{i,j-1}}{\pi_{i,j+1}}-\frac{\rho_{i,j}}{\pi_{i,j}}\right),\ \ i=1,\cdots,N,\ j=2,\cdots,M-1.
\end{aligned} \tag{A.3}$$

(iv) Impose the no-flux boundary condition

$$F^{\mathrm{L}}_{1,j}=F^{\mathrm{R}}_{N,j}=0,\quad j=1,\cdots,M;\quad F^{\mathrm{D}}_{i,1}=F^{\mathrm{U}}_{i,M}=0,\quad i=1,\cdots,N. \tag{A.4}$$

Then the continuous-time finite volume scheme is

$$\dot{\rho}_{i,j}\Delta x\Delta y=F^{\mathrm{R}}_{i,j}+F^{\mathrm{L}}_{i,j}+F^{\mathrm{U}}_{i,j}+F^{\mathrm{D}}_{i,j} \tag{A.5}$$

for $i=1,\cdots,N, j=1,\cdots,M$ with the no-flux boundary condition (A.4). Here $\dot{\rho}_{i,j}$ refers to the time derivative of $\rho_{i,j}$. Denote $g_{i,j}:=\frac{\rho_{i,j}}{\pi_{i,j}}$. Recast (A.5) as a five-point scheme

$$\begin{aligned}
\pi_{i,j}\dot{g}_{i,j}=&\frac{1}{\Delta x^2}\left(\frac{D(\pi_{i+1,j}+\pi_{i,j})}{2}+\Delta x(\boldsymbol{u}\cdot\boldsymbol{n})^{R-}_{i,j}\right)g_{i+1,j}\\
&+\frac{1}{\Delta x^2}\left(\frac{D(\pi_{i-1,j}+\pi_{i,j})}{2}+\Delta x(\boldsymbol{u}\cdot\boldsymbol{n})^{L-}_{i,j}\right)g_{i-1,j}\\
&+\frac{1}{\Delta y^2}\left(\frac{D(\pi_{i,j+1}+\pi_{i,j})}{2}+\Delta y(\boldsymbol{u}\cdot\boldsymbol{n})^{U-}_{i,j}\right)g_{i,j+1}\\
&+\frac{1}{\Delta y^2}\left(\frac{D(\pi_{i,j-1}+\pi_{i,j})}{2}+\Delta y(\boldsymbol{u}\cdot\boldsymbol{n})^{D-}_{i,j}\right)g_{i,j-1}-\lambda_{i,j}g_{i,j},\\
\lambda_{i,j}:=&\frac{D(\pi_{i+1,j}+2\pi_{i,j}+\pi_{i-1,j})}{2\Delta x^2}+\frac{D(\pi_{i,j+1}+2\pi_{i,j}+\pi_{i,j-1})}{2\Delta y^2}\\
&+\frac{(\boldsymbol{u}\cdot\boldsymbol{n})^{R-}_{i,j}+(\boldsymbol{u}\cdot\boldsymbol{n})^{L-}_{i,j}}{\Delta x}+\frac{(\boldsymbol{u}\cdot\boldsymbol{n})^{U-}_{i,j}+(\boldsymbol{u}\cdot\boldsymbol{n})^{D-}_{i,j}}{\Delta y}.
\end{aligned}$$

Following the idea for the unconditionally stable explicit scheme (3.35), choose constant $a>\max_{i,j}\frac{\lambda_{i,j}}{\pi_{i,j}}$. Using constant $a>0$, we can construct an unconditionally stable explicit scheme, which can be regarded as a new Markov chain with a transition probability $\tilde{K}^*$. With Q defined in (2.29), the time discretization is

$$\frac{\rho^{k+1}-\rho^k}{\Delta t}=Q^*\rho^k+a(\rho^k-\rho^{k+1}). \tag{A.6}$$

Thus the transition probability $\tilde{K}^*$ is given by

$$\rho^{k+1}=\tilde{K}^*\rho^k,\quad \tilde{K}^*:=I+\frac{\Delta tQ^*}{1+a\Delta t},\quad \sum_j\tilde{K}_{ij}=1,\quad \tilde{K}_{ij}\geq 0. \tag{A.7}$$

Notice we have chosen $\boldsymbol{u}$ satisfying (2.36) and thus the equivalent flux F_{ji} in (2.39) still defines a stochastic Q-matrix. With the notation $g_{i,j}=\frac{\rho_{ij}}{\pi_{i,j}}$, (A.7) reads as three parts:

interiors, four sides, and four corners. For interior cells $i=2,\cdots,N-1$, $j=2,\cdots,M-1$:

$$\begin{aligned}\rho_{i,j}^{k+1}=&\frac{\Delta t}{(1+a\Delta t)\Delta x^2}\left(\frac{D(\pi_{i+1,j}+\pi_{i,j})}{2}+\Delta x(\boldsymbol{u}\cdot\boldsymbol{n})_{i,j}^{R-}\right)g_{i+1,j}^k\\&+\frac{\Delta t}{(1+a\Delta t)\Delta x^2}\left(\frac{D(\pi_{i-1,j}+\pi_{i,j})}{2}+\Delta x(\boldsymbol{u}\cdot\boldsymbol{n})_{i,j}^{L-}\right)g_{i-1,j}^k\\&+\frac{\Delta t}{(1+a\Delta t)\Delta y^2}\left(\frac{D(\pi_{i,j+1}+\pi_{i,j})}{2}+\Delta y(\boldsymbol{u}\cdot\boldsymbol{n})_{i,j}^{U-}\right)g_{i,j+1}^k\\&+\frac{\Delta t}{(1+a\Delta t)\Delta y^2}\left(\frac{D(\pi_{i,j-1}+\pi_{i,j})}{2}+\Delta y(\boldsymbol{u}\cdot\boldsymbol{n})_{i,j}^{D-}\right)g_{i,j-1}^k\\&+\frac{\pi_{i,j}+\Delta t(a\pi_{i,j}-\lambda_{i,j})}{1+a\Delta t}g_{i,j}^k.\end{aligned}\tag{A.8}$$

For left side cells $i=1$, $j=2,\cdots,M-1$:

$$\begin{aligned}\rho_{1,j}^{k+1}=&\frac{\Delta t}{(1+a\Delta t)\Delta x^2}\left(\frac{D(\pi_{2,j}+\pi_{1,j})}{2}+\Delta x(\boldsymbol{u}\cdot\boldsymbol{n})_{1,j}^{R-}\right)g_{2,j}^k\\&+\frac{\Delta t}{(1+a\Delta t)\Delta y^2}\left(\frac{D(\pi_{1,j+1}+\pi_{1,j})}{2}+\Delta y(\boldsymbol{u}\cdot\boldsymbol{n})_{1,j}^{U-}\right)g_{1,j+1}^k\\&+\frac{\Delta t}{(1+a\Delta t)\Delta y^2}\left(D\frac{(\pi_{1,j-1}+\pi_{1,j})}{2}+\Delta y(\boldsymbol{u}\cdot\boldsymbol{n})_{1,j}^{D-}\right)g_{1,j-1}^k+\frac{\pi_{1,j}+\Delta t(a\pi_{1,j}-\lambda_{1,j})}{1+a\Delta t}g_{1,j}^k,\\\lambda_{1,j}:=&\frac{D(\pi_{2,j}+\pi_{1,j})}{2\Delta x^2}+\frac{D(\pi_{1,j+1}+2\pi_{1,j}+\pi_{1,j-1})}{2\Delta y^2}+\frac{(\boldsymbol{u}\cdot\boldsymbol{n})_{1,j}^{R-}}{\Delta x}+\frac{(\boldsymbol{u}\cdot\boldsymbol{n})_{1,j}^{U-}+(\boldsymbol{u}\cdot\boldsymbol{n})_{1,j}^{D-}}{\Delta y}.\end{aligned}\tag{A.9}$$

Similar for the right, down and up side cells.

For left-down corner cell $i=1$, $j=1$:

$$\begin{aligned}\rho_{1,1}^{k+1}=&\frac{\Delta t}{(1+a\Delta t)\Delta x^2}\left(\frac{D(\pi_{2,1}+\pi_{1,1})}{2}+\Delta x(\boldsymbol{u}\cdot\boldsymbol{n})_{1,1}^{R-}\right)g_{2,1}^k\\&+\frac{\Delta t}{(1+a\Delta t)\Delta y^2}\left(\frac{D(\pi_{1,2}+\pi_{1,1})}{2}+\Delta y(\boldsymbol{u}\cdot\boldsymbol{n})_{1,1}^{U-}\right)g_{1,2}^k+\frac{\pi_{1,1}+\Delta t(a\pi_{1,1}-\lambda_{1,1})}{1+a\Delta t}g_{1,1}^k,\\\lambda_{1,1}:=&\frac{D(\pi_{2,1}+\pi_{1,1})}{2\Delta x^2}+\frac{D(\pi_{1,2}+\pi_{1,1})}{2\Delta y^2}+\frac{(\boldsymbol{u}\cdot\boldsymbol{n})_{1,1}^{R-}}{\Delta x}+\frac{(\boldsymbol{u}\cdot\boldsymbol{n})_{1,1}^{U-}}{\Delta y}.\end{aligned}\tag{A.10}$$

Similar for the left-up, right-down and right-up corner cells.

A.2 Upwind scheme in 2D for general irreversible process

Take a 2D domain as $\Omega:=[a,b]\times[c,d]$. We present the upwind scheme (2.6) based on structured grids for a Fokker-Planck equation on the 2D domain Ω. Let the grid size be $\Delta x=\frac{b-a}{N}$, $\Delta y=\frac{d-c}{M}$.

(i) Define the rectangle cells and cell centers as (A.1), and (A.2).

(ii) Denote the drift $\boldsymbol{b}=:(u,v)$ of cell C_{ij} on the bisection point on edges as

$$u_{i\pm\frac{1}{2},j}=u\Big(x_i\pm\frac{1}{2}\Delta x,y_j\Big),\quad v_{i,j\pm\frac{1}{2}}=v\Big(x_i,y_j\pm\frac{1}{2}\Delta y\Big); \tag{A.11}$$

(iii) Based on (2.6), define the inward flux F into cell C_{ij} from four cell faces as

$$\begin{aligned}
F^{\mathrm{R}}_{i,j}&=\Delta y\left(\frac{D(\rho_{i+1,j}-\rho_{i,j})}{\Delta x}+u^-_{i+\frac{1}{2},j}\rho_{i+1,j}-u^+_{i+\frac{1}{2},j}\rho_{i,j}\right),\\
F^{\mathrm{L}}_{i,j}&=\Delta y\left(\frac{D(\rho_{i-1,j}-\rho_{i,j})}{\Delta x}+u^+_{i-\frac{1}{2},j}\rho_{i-1,j}-u^-_{i-\frac{1}{2},j}\rho_{i,j}\right),\ \ i=2,\cdots,N-1,\ j=1,\cdots,M;\\
F^{\mathrm{U}}_{i,j}&=\Delta x\left(\frac{D(\rho_{i,j+1}-\rho_{i,j})}{\Delta y}+v^-_{i,j+\frac{1}{2}}\rho_{i,j+1}-v^+_{i,j+\frac{1}{2}}\rho_{i,j}\right),\\
F^{\mathrm{D}}_{i,j}&=\Delta x\left(\frac{D(\rho_{i,j-1}-\rho_{i,j})}{\Delta y}+v^+_{i,j-\frac{1}{2}j}\rho_{i,j-1}-v^-_{i,j-\frac{1}{2}}\rho_{i,j}\right),\ \ i=1,\cdots,N,\ j=2,\cdots,M-1.
\end{aligned} \tag{A.12}$$

(iv) Impose the no-flux boundary condition

$$F^{\mathrm{L}}_{1,j}=F^{\mathrm{R}}_{N,j}=0,\quad j=1,\cdots,M;\quad F^{\mathrm{D}}_{i,1}=F^{\mathrm{U}}_{i,M}=0,\quad i=1,\cdots,N. \tag{A.13}$$

Then the continuous-time finite volume scheme is

$$\dot\rho_{i,j}\Delta x\Delta y=F^{\mathrm{R}}_{i,j}+F^{\mathrm{L}}_{i,j}+F^{\mathrm{U}}_{i,j}+F^{\mathrm{D}}_{i,j} \tag{A.14}$$

for $i=1,\cdots,N, j=1,\cdots,M$ with the no-flux boundary condition (A.13). Here $\dot\rho_{i,j}$ refers to the time derivative of $\rho_{i,j}$. Recast (A.14) as a five-point scheme

$$\begin{aligned}
\dot\rho_{i,j}=&\frac{1}{\Delta x^2}\left(D+\Delta x u^-_{i+\frac{1}{2},j}\right)\rho_{i+1,j}+\frac{1}{\Delta x^2}\left(D+\Delta x u^+_{i-\frac{1}{2},j}\right)\rho_{i-1,j}\\
&+\frac{1}{\Delta y^2}\left(D+\Delta y v^-_{i,j+\frac{1}{2}}\right)\rho_{i,j+1}+\frac{1}{\Delta y^2}\left(D+\Delta y v^+_{i,j-\frac{1}{2}}\right)\rho_{i,j-1}-\lambda_{i,j}\rho_{i,j},\\
\lambda_{i,j}:=&\frac{2D}{\Delta x^2}+\frac{2D}{\Delta y^2}+\frac{u^+_{i+\frac{1}{2},j}+u^-_{i-\frac{1}{2},j}}{\Delta x}+\frac{v^+_{i,j+\frac{1}{2}}+v^-_{i,j-\frac{1}{2}}}{\Delta y}.
\end{aligned}$$

Following the unconditionally stable explicit scheme (3.35), define $a:=\max_{i,j}\lambda_{i,j}$. Then (3.35) reads as three parts: interiors, four sides, and four corners.

For interior cells $i=2,\cdots,N-1$, $j=2,\cdots,M-1$:

$$\begin{aligned}\rho_{i,j}^{k+1}=&\frac{\Delta t}{(1+a\Delta t)\Delta x^2}\left(D+\Delta x u_{i+\frac{1}{2},j}^{-}\right)\rho_{i+1,j}^{k}+\frac{\Delta t}{(1+a\Delta t)\Delta x^2}\left(D+\Delta x u_{i-\frac{1}{2},j}^{+}\right)\rho_{i-1,j}^{k}\\&+\frac{\Delta t}{(1+a\Delta t)\Delta y^2}\left(D+\Delta y v_{i,j+\frac{1}{2}}^{-}\right)\rho_{i,j+1}^{k}+\frac{\Delta t}{(1+a\Delta t)\Delta y^2}\left(D+\Delta y v_{i,j-\frac{1}{2}}^{+}\right)\rho_{i,j-1}^{k}\\&+\frac{1+\Delta t(a-\lambda_{i,j})}{1+a\Delta t}\rho_{i,j}^{k},\\\lambda_{i,j}:=&\frac{2D}{\Delta x^2}+\frac{2D}{\Delta y^2}+\frac{u_{i+\frac{1}{2},j}^{+}+u_{i-\frac{1}{2},j}^{-}}{\Delta x}+\frac{v_{i,j+\frac{1}{2}}^{+}+v_{i,j-\frac{1}{2}}^{-}}{\Delta y}.\end{aligned}\tag{A.15}$$

For left side cells $i=1$, $j=2,\cdots,M-1$:

$$\begin{aligned}\rho_{1,j}^{k+1}=&\frac{\Delta t}{(1+a\Delta t)\Delta x^2}\left(D+\Delta x u_{\frac{3}{2},j}^{-}\right)\rho_{2,j}^{k}+\frac{\Delta t}{(1+a\Delta t)\Delta y^2}\left(D+\Delta y v_{1,j+\frac{1}{2}}^{-}\right)\rho_{1,j+1}^{k}\\&+\frac{\Delta t}{(1+a\Delta t)\Delta y^2}\left(D+\Delta y v_{1,j-\frac{1}{2}}^{+}\right)\rho_{1,j-1}^{k}+\frac{1+\Delta t(a-\lambda_{i,j})}{1+a\Delta t}\rho_{i,j}^{k},\\\lambda_{1,j}:=&\frac{D}{\Delta x^2}+\frac{2D}{\Delta y^2}+\frac{u_{\frac{3}{2},j}^{+}}{\Delta x}+\frac{v_{1,j+\frac{1}{2}}^{+}+v_{1,j-\frac{1}{2}}^{-}}{\Delta y}.\end{aligned}\tag{A.16}$$

Similar for the right, down and up side cells.

For left-down corner cell $i=1$, $j=1$:

$$\begin{aligned}\rho_{1,1}^{k+1}=&\frac{\Delta t}{(1+a\Delta t)\Delta x^2}\left(D+\Delta x u_{\frac{3}{2},1}^{-}\right)\rho_{2,1}^{k}+\frac{\Delta t}{(1+a\Delta t)\Delta y^2}\left(D+\Delta y v_{1,\frac{3}{2}}^{-}\right)\rho_{1,2}^{k}\\&+\frac{1+\Delta t(a-\lambda_{1,1})}{1+a\Delta t}\rho_{i,j}^{k},\\\lambda_{1,1}:=&\frac{D}{\Delta x^2}+\frac{D}{\Delta y^2}+\frac{u_{\frac{3}{2},1}^{+}}{\Delta x}+\frac{v_{1,\frac{3}{2}}^{+}}{\Delta y}.\end{aligned}\tag{A.17}$$

Similar for the left-up, right-down and right-up corner cells.

Remark A.1. Since this example has rectangle grids, we can also define the flux F in the x-direction and y-direction respectively

$$\begin{aligned}&F_{i-\frac{1}{2},j}=F_{i,j}^{L},\quad i=2,\cdots,N,\ \ j=1,\cdots,M,\\&F_{i,j-\frac{1}{2}}=F_{i,j}^{D},\quad i=1,\cdots,N,\ \ j=2,\cdots,M,\\&F_{\frac{1}{2},j}=F_{N+\frac{1}{2},j}=0,\quad j=1,\cdots,M,\quad F_{i,\frac{1}{2}}=F_{i,M+\frac{1}{2}}=0,\quad i=1,\cdots,N.\end{aligned}\tag{A.18}$$

Then (A.14) can be recast as

$$\dot{\rho}_{i,j}\Delta x\Delta y+F_{i+\frac{1}{2},j}-F_{i-\frac{1}{2},j}+F_{i,j+\frac{1}{2}}-F_{i,j-\frac{1}{2}}=0.\tag{A.19}$$

B Comparison between our upwind scheme with other finite volume schemes

The famous Scharfetter–Gummel(SG) scheme was first proposed in [31] for 1D semiconductor device equation and there are many mathematical analysis and extensions on it, c.f., [26, 35] and recently summarized as B-schemes in [3]. We remark it also has the Q-matrix structure and the π-symmetric decomposition. Indeed, the finite volume scheme can be reformulated as

$$\begin{aligned}\frac{\mathrm{d}}{\mathrm{d}t}\rho_i|C_i| = \sum_j \frac{D|\Gamma_{ij}|}{|\mathbf{y}_j-\mathbf{y}_i|}\left[B\left(\frac{1}{D}(\boldsymbol{b}\cdot\boldsymbol{n})_{ij}|\mathbf{y}_j-\mathbf{y}_i|\right)\rho_j - B\left(\frac{1}{D}(\boldsymbol{b}\cdot\boldsymbol{n})_{ji}|\mathbf{y}_j-\mathbf{y}_i|\right)\rho_i\right];\\ \text{Scharfetter–Gummel:}\quad B(x)=\frac{x}{e^x-1},\quad x\neq 0,\quad B(0)=1;\\ \text{Upwind scheme:}\quad B(x)=1+x^-.\end{aligned} \tag{B.1}$$

Since $B(x)>0$, then with $Q_{ji}=\frac{D|\Gamma_{ij}|}{|\mathbf{y}_j-\mathbf{y}_i||C_j|}B\left(\frac{1}{D}(\boldsymbol{b}\cdot\boldsymbol{n})_{ij}|\mathbf{y}_j-\mathbf{y}_i|\right)$, we have exactly same decomposition as (3.9). Specially, for the reversible case, let φ be the potential such that $\boldsymbol{b}=-\nabla\varphi$ and thus $\pi\propto e^{-\varphi/D}$. Take the approximation $(\boldsymbol{b}\cdot\boldsymbol{n})_{ij}|\mathbf{y}_j-\mathbf{y}_i|\approx\varphi_i-\varphi_j$, then for $B(x)=\frac{x}{e^x-1}$, one can directly verify the detailed balance condition for $\pi=e^{-\varphi_i/D}$

$$Q_{ji}\pi_j|C_j| = \frac{|\Gamma_{ij}|}{|\mathbf{y}_j-\mathbf{y}_i|}\frac{\varphi_i-\varphi_j}{e^{\varphi_i/D}-e^{\varphi_j/D}} = \frac{|\Gamma_{ij}|}{|\mathbf{y}_j-\mathbf{y}_i|}\left(\Lambda(\pi_i^{-1},\pi_j^{-1})\right)^{-1} = Q_{ij}\pi_i|C_i|,$$

where $\Lambda(x,y)=\frac{x-y}{\log x-\log y}$ is the so-called logarithmic mean. Hence in (3.9), $F_{ji}^{\pi}=0$ while the symmetric coefficient α_{ij} in (3.9) then becomes

$$\alpha_{ij}=Q_{ji}\pi_j|C_j| = \frac{D|\Gamma_{ij}|}{|\mathbf{y}_j-\mathbf{y}_i|}\left(\int_0^1 \frac{1}{e^{-\varphi_i/D+s(\varphi_i-\varphi_j)/D}}\mathrm{d}x\right)^{-1},$$

where the average is the harmonic average of π with linear interpolation for φ along edge $[\mathbf{y}_i,\mathbf{y}_j]$; c.f. [25, 26]. If replacing the harmonic average above by the arithmetic mean of π_i and π_j, then SG scheme becomes our scheme (2.27) in the reversible case, i.e., $\boldsymbol{u}=0$ in (2.26).

C Remarks on Hill's derivation on the positive entropy production rate

We remark that HILL derives (3.12) by calculating the change of free energy individually as follows. Denote G_i as the Gibbs free energy at site i. Then the chemical potential at site i at the steady state is

$$\mu_i = G_i+\mu_M+kT\log\pi_i. \tag{C.1}$$

Here μ_M is the energy provided by the environment (heat bath in the open system) which probably has different values for different orientations of a circulation in a biochemical reaction. For instance, in a simple Enzyme-substrate-product example [19, Section 9], $\mu_M=\mu_S$ is the chemical potential of the substrate for a positive circulation, while $\mu_M=\mu_P$ is the chemical potential of the product for an opposite circulation. Then by the Arrhenius law, the transition rate from site i to site j is given by

$$\frac{Q_{ij}}{Q_{ji}}=e^{\frac{G_i-G_j+\mu_M}{kT}},\quad \mu_M=\mu_S \text{ for } i=1,\ \mu_M=-\mu_P \text{ for } j=1. \tag{C.2}$$

This together with (C.1), implies

$$\mu_i-\mu_j=kT\log\frac{Q_{ij}\pi_i}{Q_{ji}\pi_j}. \tag{C.3}$$

Thus at the steady state, the individual energy change (in the unit of energy per unit time) due to the nonzero flux $i\to j$ is always

$$F_{ij}^{\pi}\left(\mu_i-\mu_j\right)=\left(Q_{ij}\pi_i-Q_{ji}\pi_j\right)kT\log\frac{Q_{ij}\pi_i}{Q_{ji}\pi_j}\geq 0. \tag{C.4}$$

Adding each sites together and with our notation, we obtain (3.12). Using Kolmogorov's circulation criterion, we can check

$$\frac{Q_{12}Q_{23}\cdots Q_{n1}}{Q_{21}Q_{32}\cdots Q_{1n}}=e^{\frac{\mu_S-\mu_P}{kT}}\neq 1. \tag{C.5}$$

In fact, if Q satisfies Kolmogorov's circulation criterion, then by construction proof, one can define a $\pi_i:=\frac{Q_{12}Q_{23}\cdots Q_{ki}}{Q_{21}Q_{32}\cdots Q_{ik}}$ and prove it is uniquely defined and satisfies detailed balance condition $Q_{ji}\pi_j=Q_{ij}\pi_i$.

References

[1] Randolph E Bank, WM Coughran Jr, and Lawrence C Cowsar. The finite volume Scharfetter-Gummel method for steady convection diffusion equations. *Computing and Visualization in Science*, 1(3):123–136, 1998.

[2] Marianne Bessemoulin-Chatard. A finite volume scheme for convection–diffusion equations with nonlinear diffusion derived from the Scharfetter–Gummel scheme. *Numerische Mathematik*, 121(4):637–670, 2012.

[3] Claire Chainais-Hillairet and Maxime Herda. Large-time behaviour of a family of finite volume schemes for boundary-driven convection–diffusion equations. *IMA Journal of Numerical Analysis*, 40(4):2473–2504, 2020.

[4] Claire Chainais-Hillairet, Maxime Herda, Simon Lemaire, and Julien Moatti. Long-time behaviour of hybrid finite volume schemes for advection–diffusion equations: Linear and nonlinear approaches. *Numerische Mathematik*, 151(4):963–1016, 2022.

[5] Claire Chainais-Hillairet, Jian-Guo Liu, and Yue-Jun Peng. Finite volume scheme for multi-dimensional drift-diffusion equations and convergence analysis. *ESAIM: Mathematical Modelling and Numerical Analysis-Modélisation Mathématique et Analyse Numérique*, 37(2):319–338, 2003.
[6] Mu-Fa Chen. Equivalence of exponential ergodicity and L2-exponential convergence for Markov chains. *Stochastic Processes and Their Applications*, 87(2):281–297, Jun 2000.
[7] R. R. Coifman, I. G. Kevrekidis, S. Lafon, M. Maggioni, and B. Nadler. Diffusion maps, reduction coordinates, and low dimensional representation of stochastic systems. *Multiscale Modeling & Simulation*, 7(2):842–864, 2008.
[8] Peter Constantin, Alexander Kiselev, Lenya Ryzhik, and Andrej Zlatoš. Diffusion and mixing in fluid flow. *Annals of Mathematics*, pages 643–674, 2008.
[9] Weinan E and Jian-Guo Liu. Vorticity boundary condition and related issues for finite difference schemes. *Journal of Computational Physics*, 124(2):368–382, 1996.
[10] Robert Eymard, Thierry Gallouët, and Raphaèle Herbin. Finite volume methods. *Handbook of Numerical Analysis*, 7:713–1018, 2000.
[11] Albert Fannjiang and George Papanicolaou. Convection enhanced diffusion for periodic flows. *SIAM Journal on Applied Mathematics*, 54(2):333–408, 1994.
[12] Jin Feng and Thomas G Kurtz. *Large deviations for stochastic processes*. Number 131. American Mathematical Soc., 2006.
[13] Yuan Gao, Tiejun Li, Xiaoguang Li, and Jian-Guo Liu. Transition path theory for Langevin dynamics on manifold: Optimal control and data-driven solver. *Multiscale Modeling & Simulation*, 21(1):1–33, 2023.
[14] Yuan Gao and Jian-Guo Liu. A note on parametric Bayesian inference via gradient flows. *Annals of Mathematical Sciences and Applications*, 5(2):261–282, 2020.
[15] Yuan Gao and Jian-Guo Liu. Revisit of macroscopic dynamics for some non-equilibrium chemical reactions from a Hamiltonian viewpoint. *Journal of Statistical Physics*, 189(2):1–57, 2022.
[16] Yuan Gao and Jian-Guo Liu. A selection principle for weak KAM solutions via Freidlin-Wentzell large deviation principle of invariant measures. To appear in *SIAM Journal on Mathematics Analysis*.
[17] Yuan Gao and Jian-Guo Liu. Thermodynamic limit of chemical master equation via nonlinear semigroup. To appear in *Multiscale Modeling & Simulation*.
[18] Yuan Gao, Jian-Guo Liu, and Nan Wu. Data-driven efficient solvers for Langevin dynamics on manifold in high dimensions. *Applied and Computational Harmonic Analysis*, 62:261–309, 2023.
[19] T.L. Hill. *Free Energy Transduction and Biochemical Cycle Kinetics*. Dover Books on Chemistry. Dover Publications, 2005.
[20] Elton P Hsu. *Stochastic Analysis on Manifolds*, volume 38. American Mathematical Soc., 2002.
[21] Nobuyuki Ikeda and Shinzo Watanabe. *Stochastic Differential Equations and Diffusion Processes*. Amsterdam: North-Holland Pub. Co., 1981.
[22] E. M. Izhikevich and R. FitzHugh. FitzHugh-Nagumo model. *Scholarpedia*, 1(9):1349, 2006.
[23] Thomas Milton Liggett. *Continuous Time Markov Processes: An Introduction*, volume 113. American Mathematical Soc., 2010.
[24] Jian-Guo Liu and Chi-Wang Shu. A high-order discontinuous Galerkin method for 2D incompressible flows. *Journal of Computational Physics*, 160(2):577–596, 2000.
[25] Peter A Markowich. *The Stationary Semiconductor Device Equations*. Springer Science & Business Media, 1985.

[26] Peter A Markowich and Miloš A Zlámal. Inverse-average-type finite element discretizations of selfadjoint second-order elliptic problems. *Mathematics of Computation*, 51(184):431–449, 1988.
[27] Alexander Mielke, D. R. Michiel Renger, and Mark A. Peletier. On the relation between gradient flows and the large-deviation principle, with applications to Markov chains and diffusion. *Potential Analysis*, 41(4):1293–1327, Nov 2014.
[28] Lars Onsager. Reciprocal relations in irreversible processes. I. *Phys. Rev.*, 37:405–426, Feb 1931.
[29] I. Prigogine. *Introduction to Thermodynamics of Irreversible Processes*. Wiley, 1968.
[30] Hong Qian, Min Qian, and Xiang Tang. Thermodynamics of the general diffusion process: Time-reversibility and entropy production. *Journal of Statistical Physics*, 107(5):1129–1141, 2002.
[31] Donald L Scharfetter and Hermann K Gummel. Large-signal analysis of a silicon read diode oscillator. *IEEE Transactions on Electron Devices*, 16(1):64–77, 1969.
[32] André Schlichting and Christian Seis. The Scharfetter–Gummel scheme for aggregation–diffusion equations. *IMA Journal of Numerical Analysis*, 42(3):2361–2402, 2022.
[33] Nicolás Garcia Trillos and Dejan Slepčev. On the rate of convergence of empirical measures in ∞-transportation distance. *Canadian J. Math.*, 67(6):1358–1383, 2015.
[34] Subbarao Varigonda and Tryphon T Georgiou. Dynamics of relay relaxation oscillators. *IEEE Transactions on Automatic Control*, 46(1):65–77, 2001.
[35] Jinchao Xu and Ludmil Zikatanov. A monotone finite element scheme for convection-diffusion equations. *Mathematics of Computation*, 68(228):1429–1446, 1999.